

Error estimation in quantities of interest by locally equilibrated superconvergent patch recovery

O.A. González-Estrada¹ E. Nadal² J.J. Ródenas²
 P. Kerfriden¹ S.P.A. Bordas^{*1} F.J. Fuenmayor²

June 19, 2022

¹Institute of Mechanics and Advanced Materials (IMAM), Cardiff School of Engineering, Cardiff University, Queen's Buildings, The Parade, Cardiff CF24 3AA Wales, UK, e-mail: {estradaoag, kerfridenp}@cardiff.ac.uk, stephane.bordas@alum.northwestern.edu

²Centro de Investigación de Tecnología de Vehículos (CITV), Universitat Politècnica de València, E-46022-Valencia, Spain, e-mail: jjrodena@mcm.upv.es, ennaso@upv.es, ffuenmay@mcm.upv.es

Abstract

Goal-oriented error estimates (GOEE) have become popular tools to quantify and control the local error in quantities of interest (QoI), which are often more pertinent than local errors in energy for design purposes (e.g. the mean stress or mean displacement in a particular area, the stress intensity factor for fracture problems,...). These GOEE are one of the key unsolved problems of advanced engineering firms in the aerospace industry. Residual-based error estimators can be used to estimate errors in quantities of interest for finite element approximations. This work presents a recovery-based error estimation technique for QoIs whose main characteristic is the use of an enhanced version of the Superconvergent Patch Recovery (SPR) technique previously used for error estimation in the energy norm. This enhanced SPR technique is used to recover both the primal and dual solutions. It provides a nearly statically admissible stress field that results in accurate estimations of the local contributions to the discretization error in the QoI and, therefore, in an accurate estimation of this magnitude. This approach leads to a technique with reasonable computational cost that could be easily implemented into already available finite element codes.

KEY WORDS: goal-oriented, error estimation, recovery, quantities of interest, error control, mesh adaptivity

1 Introduction

Verification and quality assessment of numerical simulations is a critical area of research. Techniques to control the error in numerical simulations and verify the approximate solutions have been a subject of concern for many years. Further

development is expected to have a profound impact on the reliability and utility of simulation methods. Effective methods for assessing the global discretization error in energy have been extensively developed since the late 70s. However, controlling the error in quantities of interest to engineers, e.g. the average stress or average displacement in a given region or the stress intensity factors is not equivalent to controlling the error in energy. Yet, the widely stated need of practicing engineers is to evaluate and minimise the discretisation error in these “quantities of interest.” Less attention, however, has been given to the emerging, more advanced, “goal-oriented” error estimates. This paper is a step in this direction which provides a simple procedure to evaluate engineeringly-relevant quantities of interest.

Energy-based error estimates can be classified into different families [1, 2]: residual-based error estimators, recovery-based error estimators, dual techniques, *etc.* Residual-based error estimators originally introduced by Babuška and Rheinboldt [3] are characterised by a strong mathematical basis. To estimate the error, they consider local residuals of the numerical solution. By investigating the residuals occurring in a patch of elements or even in a single element it is possible to estimate the errors which arise locally. These methods were improved with the introduction of the *residual equilibration* by Ainsworth and Oden [1]. Recovery-based error estimates were first introduced by Zienkiewicz and Zhu [4] and are often preferred by practitioners because they are robust, simple to use and provide an enhanced solution which may be used as output. Further improvements were made with the introduction of new recovery procedures such as the superconvergent patch recovery (SPR) proposed by the same authors [5, 6] and many papers following [7, 8, 9, 10, 11, 12]. Recovery techniques were extended to enriched approximations in [13, 14, 15, 16] and to Hellinger-Reissner smoothing-based finite elements in [17] and the role of enrichment and statical admissibility in such recovery procedures discussed in [18]. Duality-based techniques rely on the evaluation of two different fields, one compatible in displacements and another equilibrated in stresses [19].

Most techniques used to obtain error estimates prior to the mid 90s were aimed to evaluate the global error in the energy norm. Nevertheless, as discussed above, the goal of numerical simulations is generally not the determination of the strain energy alone, but the reliable prediction of a particular quantity of interest (QoI) which is needed for making decisions during the design process. Therefore, it is important to guarantee the quality of such analyses by controlling the error of the approximation in terms of the QoI rather than the global energy norm. Significant advances in the late 90s introduced a new approach focused on the evaluation of error estimates of local quantities [1, 20, 21]. In order to obtain an error estimate for the QoI two different problems are solved: the primal problem which is the problem under consideration, and the dual or adjoint problem which is related to the QoI. The adjoint problem is the same as the primal problem except for the loads and boundary conditions, which are determined as a function of the QoI. Goal-oriented error estimators have been usually developed from the basis of residual formulations and the widely used strategy of solving the dual problem [1, 22]. Although limited, the use of recovery techniques to evaluate the error in quantities of interest can be found in [23, 24], and considering dual analysis in [25].

In this paper we propose to extend the recovery techniques presented in [12, 26,

15, 27] to evaluate accurate error estimates for linear QoIs. The recovery technique requires the analytical expressions of the body loads and boundary tractions which must be evaluated also for the dual problem in order to consider equilibrium conditions. In Section 2 we define the problem and the finite element approximation used. Section 3 focuses on the representation of the error in the QoIs and the solution of the dual problem. Section 4 deals with the definitions of the dual problem and describes the expressions of body loads and boundary tractions required for the stress recovery of the dual problem for different linear QoI. In Section 5 we introduce the nearly equilibrated recovery technique used to obtain enhanced stress fields for both the primal and dual solutions. In Section 6 we present some numerical results and, finally, conclusions are drawn in Section 7.

2 Problem statement and solution

In this section, we briefly present the model for the 2D linear elasticity problem. Denote, in vectorial form, $\boldsymbol{\sigma}$ and $\boldsymbol{\varepsilon}$ as the stresses and strains, \mathbf{D} as the elasticity matrix of the constitutive relation $\boldsymbol{\sigma} = \mathbf{D}\boldsymbol{\varepsilon}$, and the unknown displacement field \mathbf{u} , which values in $\Omega \subset \mathbb{R}^2$. \mathbf{u} is the solution of the boundary value problem given by

$$-\nabla \cdot \boldsymbol{\sigma}(\mathbf{u}) = \mathbf{b} \quad \text{in } \Omega \quad (1)$$

$$\boldsymbol{\sigma}(\mathbf{u}) \cdot \mathbf{n} = \mathbf{t} \quad \text{on } \Gamma_N \quad (2)$$

$$\mathbf{u} = \bar{\mathbf{u}} \quad \text{on } \Gamma_D, \quad (3)$$

where Γ_N and Γ_D denote the Neumann and Dirichlet boundaries with $\partial\Omega = \overline{\Gamma_N \cup \Gamma_D}$ and $\Gamma_N \cap \Gamma_D = \emptyset$, \mathbf{b} are body loads and \mathbf{t} are the tractions imposed along Γ_N .

Consider the initial stresses $\boldsymbol{\sigma}_0$ and strains $\boldsymbol{\varepsilon}_0$, the symmetric bilinear form $a : (V + \bar{\mathbf{u}}) \times V \rightarrow \mathbb{R}$ and the continuous linear form $\ell : V \rightarrow \mathbb{R}$ are defined by

$$a(\mathbf{u}, \mathbf{v}) := \int_{\Omega} \boldsymbol{\sigma}^T(\mathbf{u}) \boldsymbol{\varepsilon}(\mathbf{v}) d\Omega = \int_{\Omega} \boldsymbol{\sigma}^T(\mathbf{u}) \mathbf{D}^{-1} \boldsymbol{\sigma}(\mathbf{v}) d\Omega \quad (4)$$

$$\ell(\mathbf{v}) := \int_{\Omega} \mathbf{v}^T \mathbf{b} d\Omega + \int_{\Gamma_N} \mathbf{v}^T \mathbf{t} d\Gamma + \int_{\Omega} \boldsymbol{\sigma}^T(\mathbf{v}) \boldsymbol{\varepsilon}_0 d\Omega - \int_{\Omega} \boldsymbol{\varepsilon}^T(\mathbf{v}) \boldsymbol{\sigma}_0 d\Omega. \quad (5)$$

With these notations, the variational form of the problem reads [28]

$$\text{Find } \mathbf{u} \in (V + \bar{\mathbf{u}}) : \forall \mathbf{v} \in V \quad a(\mathbf{u}, \mathbf{v}) = \ell(\mathbf{v}) \quad (6)$$

where V is the standard test space for the elasticity problem such that $V = \{\mathbf{v} \mid \mathbf{v} \in [H^1(\Omega)]^2, \mathbf{v}|_{\Gamma_D}(\mathbf{x}) = \mathbf{0}\}$.

Let \mathbf{u}^h be a finite element approximation of \mathbf{u} . The solution for the discrete counterpart of the variational problem in (6) lies in a subspace $(V^h + \bar{\mathbf{u}}) \subset (V + \bar{\mathbf{u}})$ associated with a mesh of finite elements of characteristic size h , and it is such that

$$\forall \mathbf{v}^h \in V^h \subset V \quad a(\mathbf{u}^h, \mathbf{v}^h) = \ell(\mathbf{v}^h) \quad (7)$$

3 Error control

3.1 Error representation

In this section we define a general framework for goal-oriented error analysis. First, we assume that the finite element discretization error is given by $\mathbf{e} = \mathbf{u} - \mathbf{u}^h$. To quantify the quality of \mathbf{u}^h in terms of \mathbf{e} different methods have been proposed, generally based on the energy norm $\|\mathbf{e}\|$ induced by $\sqrt{a(\mathbf{e}, \mathbf{e})}$ and written as

$$\|\mathbf{e}\|^2 = \int_{\Omega} (\boldsymbol{\sigma} - \boldsymbol{\sigma}^h)^T \mathbf{D}^{-1} (\boldsymbol{\sigma} - \boldsymbol{\sigma}^h) d\Omega. \quad (8)$$

where $\boldsymbol{\sigma}$ and $\boldsymbol{\sigma}^h$ represent the exact and finite element stress fields, respectively. Following Zienkiewicz-Zhu [4], an estimate of the error $\|\mathbf{e}_{es}\|$ can be formulated in the context of FE elasticity problems by introducing the approximation

$$\|\mathbf{e}\|^2 \approx \|\mathbf{e}_{es}\|^2 = \int_{\Omega} (\boldsymbol{\sigma}^* - \boldsymbol{\sigma}^h)^T \mathbf{D}^{-1} (\boldsymbol{\sigma}^* - \boldsymbol{\sigma}^h) d\Omega, \quad (9)$$

where $\boldsymbol{\sigma}^*$ represents the recovered stress field, which is a better approximation to the exact solution than $\boldsymbol{\sigma}^h$. Similarly, local element contributions can be evaluated from (9) considering the domain Ω_e of element e .

The error estimate measured in the energy norm as given in (9) can overestimate or underestimate the exact error although it is asymptotically exact¹ provided that $\boldsymbol{\sigma}^*$ has a higher convergence rate than the FE solution. In order to improve the quality of our recovery-based estimate it is useful to include the error bounding property. Recently, Díez *et al.* [26] and Ródenas *et al.* [27] have presented a methodology to obtain practical upper bounds of the error in the energy norm $\|\mathbf{e}\|$ using an SPR-based approach where equilibrium was locally imposed on each patch. The recovered stresses obtained with this technique were proven to provide very accurate estimations of the error in the energy norm.

Note that we have followed here the definition of *error estimates* provided in References [4, 7, 29] and that we reserve the term *error bounding* for techniques which provide upper or lower bounds of the error. The semantics used in Mathematics refer to (9) as an error indicator and any technique providing bounds as an error estimator.

3.2 Error in quantities of interest: duality technique

In this section we show how error estimators measured in the energy norm may be utilised to estimate the error in a particular quantity of interest [1]. The strategy consists in solving a primal problem, which is the problem at hand, and a dual problem useful to extract information on the quantity of interest (identical to the primal problem except for the applied boundary conditions and internal loads). From the FE solutions of both problems it is possible to estimate the contribution of each of the elements to the error in the QoI. This error measure allows to adapt

¹the approximate error tends towards the exact error

the mesh using procedures similar to traditional techniques based on the estimated error in the energy norm.

Consider the linear elasticity problem given in (6) and its approximate FE solution \mathbf{u}^h . For the sake of simplicity let us assume homogeneous Dirichlet boundary conditions in this problem. This problem is related to the original problem to be solved, that henceforth will be called the *primal problem*.

Let us define $Q : V \rightarrow \mathbb{R}$ as a bounded linear functional representing some quantity of interest, acting on the space V of admissible functions for the problem at hand. The goal is to estimate the error in functional Q when calculated using the value of the approximate solution \mathbf{u}^h as opposed to the exact solution \mathbf{u} :

$$Q(\mathbf{u}) - Q(\mathbf{u}^h) = Q(\mathbf{u} - \mathbf{u}^h) = Q(\mathbf{e}). \quad (10)$$

As will be shown later, $Q(\mathbf{v})$ may be interpreted as the work associated with a displacement field \mathbf{v} and a distribution of loads specific to each type of quantity of interest. If we particularize $Q(\mathbf{v})$ for $\mathbf{v} = \mathbf{u}$, this force distribution will allow to extract information concerning the quantity of interest associated with the solution of the problem in (6).

A standard procedure to evaluate $Q(\mathbf{e})$ consists in solving the auxiliary *dual* problem (also called *adjoint* or *extraction* problem) defined as:

$$\text{Find } \mathbf{w}_Q \in (V + \bar{\mathbf{w}}_Q) : \forall \mathbf{v} \in V \quad a(\mathbf{v}, \mathbf{w}_Q) = Q(\mathbf{v}). \quad (11)$$

An exact representation for the error $Q(\mathbf{e})$ in terms of the solution of the dual problem can be simply obtained by substituting $\mathbf{v} = \mathbf{e}$ in (11) and remarking that in case $\bar{\mathbf{w}}_Q = 0$, for all $\mathbf{w}_Q^h \in V^h$, due to the Galerkin orthogonality, $a(\mathbf{e}, \mathbf{w}_Q^h) = 0$ so that

$$Q(\mathbf{e}) = a(\mathbf{e}, \mathbf{w}_Q) = a(\mathbf{e}, \mathbf{w}_Q) - a(\mathbf{e}, \mathbf{w}_Q^h) = a(\mathbf{e}, \mathbf{w}_Q - \mathbf{w}_Q^h) = a(\mathbf{e}, \mathbf{e}_Q). \quad (12)$$

Therefore, the error in evaluating $Q(\mathbf{u})$ using \mathbf{u}^h is given by

$$Q(\mathbf{u}) - Q(\mathbf{u}^h) = Q(\mathbf{e}) = a(\mathbf{e}, \mathbf{e}_Q) = \int_{\Omega} (\boldsymbol{\sigma}_p - \boldsymbol{\sigma}_p^h) \mathbf{D}^{-1} (\boldsymbol{\sigma}_d - \boldsymbol{\sigma}_d^h) \, d\Omega \quad (13)$$

where $\boldsymbol{\sigma}_p$ is the stress field associated with the primal solution and $\boldsymbol{\sigma}_d$ is the one associated with the dual solution.

Following [24] we can introduce a first coarse upper bound for the global error in the QoI employing the Cauchy–Schwarz inequality that results in:

$$Q(\mathbf{e}) = a(\mathbf{e}, \mathbf{e}_Q) \leq \|\mathbf{e}\| \|\mathbf{e}_Q\| \quad (14)$$

Then, the evaluation of the error in the QoI is now expressed in terms of the error in the energy norm for the dual and primal solutions, for which several techniques are already available. However, this upper bound is rather conservative due to the use of the Cauchy–Schwarz inequality [24]. Moreover, it does not provide a local indicator that can be used to guide the adaptivity process.

For a discretization with n_e elements let us consider the local test space $V_e = \{\mathbf{v}|_{\Omega_e} : \mathbf{v} \in V\}$ and $a_e : V_e \times V_e \rightarrow \mathbb{R}$ as the associated bilinear form a to an element $\Omega_e : \Omega = \bigcup_{n_e} \Omega_e$ such that

$$\forall \mathbf{u}, \mathbf{v} \in V \quad a(\mathbf{u}, \mathbf{v}) = \sum_{n_e} a_e(\mathbf{u}, \mathbf{v}) \quad (15)$$

To obtain sharper error measures and local indicators, we can decouple the element contributions as shown in [24] such that:

$$Q(\mathbf{e}) = a(\mathbf{e}, \mathbf{e}_Q) = \sum_{n_e} a_e(\mathbf{e}, \mathbf{e}_Q) \quad \text{from(12)} \quad (16a)$$

$$\leq \sum_{n_e} |a_e(\mathbf{e}, \mathbf{e}_Q)| \quad (16b)$$

$$\leq \sum_{n_e} \|\mathbf{e}\|_{\Omega_e} \|\mathbf{e}_Q\|_{\Omega_e} \quad (16c)$$

$$\leq \|\mathbf{e}\| \|\mathbf{e}_Q\| \quad (16d)$$

Note that in (13) and the indicators derived afterwards, the error in the QoI is related to the errors in the FE approximations \mathbf{u}^h and \mathbf{w}_Q^h . On that account, any of the available procedures to estimate the error in the energy norm may be considered to obtain estimates of the error in the quantity of interest.

Similarly from (8) to (9), we can derive an estimate of the error in the QoI from (13) which reads

$$Q(\mathbf{e}) \approx Q(\mathbf{e}_{es}) = \int_{\Omega} (\boldsymbol{\sigma}_p^* - \boldsymbol{\sigma}_p^h) \mathbf{D}^{-1} (\boldsymbol{\sigma}_d^* - \boldsymbol{\sigma}_d^h) \, d\Omega \quad (17)$$

where $\boldsymbol{\sigma}_p^*$ and $\boldsymbol{\sigma}_d^*$ represent the recovered stress fields for the primal and dual problems. Here, we expect that the more accurate the recovered stress fields $\boldsymbol{\sigma}_p^*$ and $\boldsymbol{\sigma}_d^*$, the more accurate the estimation of the local contributions to the global error (this is of special interest in goal-oriented adaptivity) and the sharper the error estimate in the quantity of interest.

In order to obtain accurate representations of the exact stress fields both for the primal and dual solutions, we propose the use of the locally equilibrated recovery techniques introduced in [12, 15, 27] and described in Section 5. This technique, which is an enhancement of the superconvergent patch recovery (SPR) proposed in [5], enforces the fulfilment of the internal and boundary equilibrium equations locally on patches. For problems with singularities the stress field is also decomposed into two parts: smooth and singular, which are separately recovered.

Continuing with the ideas in [24], and using the recovery technique to obtain accurate estimates of the error with the decoupled approach, we can formulate using

(16) the following error indicators:

$$Q(\mathbf{e}) \approx Q(\mathbf{e}_{es}) = \mathcal{E}_1 = \sum_{n_e} a_e(\mathbf{e}_{es}, \mathbf{e}_{Q,es}) \quad (18a)$$

$$\leq \mathcal{E}_2 := \sum_{n_e} |a_e(\mathbf{e}_{es}, \mathbf{e}_{Q,es})| \quad (18b)$$

$$\leq \mathcal{E}_3 := \sum_{n_e} \|\mathbf{e}_{es}\|_{\Omega_e} \|\mathbf{e}_{Q,es}\|_{\Omega_e} \quad (18c)$$

$$\leq \mathcal{E}_4 := \|\mathbf{e}_{es}\| \|\mathbf{e}_{Q,es}\| \quad (18d)$$

The properties of these error estimates are discussed in [24] in more detail. In a general sense, the idea is that the more accurate the estimate, the less guaranteed is the upper bound property. The only guaranteed upper error bound is given by (18d), under the assumption that the recovery technique correctly enforces equilibrium conditions and provides upper error bounds in the energy norm for both the primal and dual solutions [26]. These indicators are shown in the numerical results for comparison.

4 Analytical definitions for the dual problem

The recovery procedure based on the SPR technique denoted as SPR-CX, and described in [12, 15, 26, 27], relies on the *a priori* knowledge of functions \mathbf{b} and \mathbf{t} to impose the internal and boundary equilibrium equations. For the primal problem these values (\mathbf{b}_p and \mathbf{t}_p) are already at hand, as seen in (1, 2), but for the dual problem they are not readily available. In this Section we present a compilation of procedures to obtain the analytical dual loads for a few typical linear quantities of interest, such as the mean values of displacements and stresses in a sub-domain of interest Ω_i . Basic compilations have been presented in [30, 31] and, in the same line, in [32], where the authors defined relations between the natural quantities of interest and dual loading data. Here, we have also included other cases like the evaluation of dual loads when the quantity of interest is the generalized stress intensity factor (GSIF).

4.1 Mean displacement in Ω_i

Let us assume that the objective is to evaluate the mean value of the displacements along the direction α in a sub-domain of interest $\Omega_i \subset \Omega$. The functional for the quantity of interest can be written as:

$$Q(\mathbf{u}) = \bar{u}_\alpha|_{\Omega_i} = \frac{1}{|\Omega_i|} \int_{\Omega_i} \mathbf{u}^T \mathbf{c}_{u_\alpha} d\Omega \quad (19)$$

where $|\Omega_i|$ is the volume of Ω_i and \mathbf{c}_{u_α} is a vector used to select the appropriate combination of components of \mathbf{u} . For example, $\mathbf{c}_{u_\alpha} = \{1, 0\}^T$ if α is parallel to the x -axis. Now, considering $\mathbf{v} \in V$ in (19) results in:

$$Q(\mathbf{v}) = \int_{\Omega_i} \mathbf{v}^T \left(\frac{\mathbf{c}_{u_\alpha}}{|\Omega_i|} \right) d\Omega = \int_{\Omega_i} \mathbf{v}^T \mathbf{b}_d d\Omega \quad (20)$$

Note that the term $\mathbf{c}_{u_\alpha}/|\Omega_i|$ formally corresponds to a vector of body forces in the problem defined in (6). Therefore, we can interpret $\mathbf{b}_d = \mathbf{c}_{u_\alpha}/|\Omega_i|$ as a constant vector of body loads applied within the sub-domain of interest Ω_i which can be used in the dual problem to extract the mean displacements.

4.2 Mean displacement along Γ_i

For the case where the quantity of interest is the functional that evaluates the mean value of the displacements along a subset Γ_i of the Neumann boundary Γ_N the expression reads:

$$Q(\mathbf{u}) = \bar{u}_\alpha|_{\Gamma_i} = \frac{1}{|\Gamma_i|} \int_{\Gamma_i} \mathbf{u}^T \mathbf{c}_{u_\alpha} d\Gamma \quad (21)$$

$|\Gamma_i|$ being the length of Γ_i and \mathbf{c}_{u_α} a Boolean vector used to select the appropriate component of \mathbf{u} . Again, considering $\mathbf{v} \in V$ in (21) we have:

$$Q(\mathbf{v}) = \int_{\Gamma_i} \mathbf{v}^T \left(\frac{\mathbf{c}_{u_\alpha}}{|\Gamma_i|} \right) d\Gamma = \int_{\Gamma_i} \mathbf{v}^T \mathbf{t}_d d\Gamma \quad (22)$$

Note that the term $\mathbf{c}_{u_\alpha}/|\Gamma_i|$ can be interpreted as a vector of tractions applied along the boundary in the problem defined in (6). Thus, $\mathbf{t}_d = \mathbf{c}_{u_\alpha}/|\Gamma_i|$ is a vector of tractions applied on Γ_i and that can be used in the dual problem to extract the mean displacements along Γ_i .

4.3 Mean strain in Ω_i

In this case we are dealing with the first derivatives of displacements. Consider for instance the component ϵ_{xx} . This term can be expressed as:

$$\epsilon_{xx} = \frac{\partial u_x}{\partial x} = \left\{ \frac{\partial}{\partial x} \frac{\partial}{\partial y} \right\} \begin{Bmatrix} u \\ 0 \end{Bmatrix} = \nabla \cdot \begin{Bmatrix} u \\ 0 \end{Bmatrix} = \nabla \cdot \left(\begin{bmatrix} 1 & 0 \\ 0 & 0 \end{bmatrix} \begin{Bmatrix} u_x \\ u_y \end{Bmatrix} \right) = \nabla \cdot (\mathbf{C}_{xx} \mathbf{u}) \quad (23)$$

Operating similarly for the other components of the strain vector we would have:

$$\epsilon_{yy} = \nabla \cdot (\mathbf{C}_{yy} \mathbf{u}) \quad \epsilon_{xy} = \nabla \cdot (\mathbf{C}_{xy} \mathbf{u}) \quad (24)$$

Taking (24), the mean value of the strain ϵ_{xx} in Ω_i can be evaluated as:

$$Q(\mathbf{u}) = \bar{\epsilon}_{xx}|_{\Omega_i} = \frac{1}{|\Omega_i|} \int_{\Omega_i} \epsilon_{xx} d\Omega = \frac{1}{|\Omega_i|} \int_{\Omega_i} \nabla \cdot (\mathbf{C}_{xx} \mathbf{u}) d\Omega \quad (25)$$

Assuming that \mathbf{u} is such that we can apply the divergence theorem the previous equation can be written as:

$$Q(\mathbf{u}) = \bar{\epsilon}_{xx}|_{\Omega_i} = \frac{1}{|\Omega_i|} \int_{\Gamma_i} (\mathbf{C}_{xx} \mathbf{u})^T \mathbf{n} d\Gamma \quad (26)$$

where \mathbf{n} is the unit outward normal vector. The domain integral is then transformed into a contour integral. Finally, choosing $\mathbf{v} \in V$ instead of \mathbf{u} in the previous expression and reordering we obtain:

$$Q(\mathbf{v}) = \int_{\Gamma_i} \mathbf{v}^T \left(\frac{\mathbf{C}_{xx}^T \mathbf{n}}{|\Omega_i|} \right) d\Gamma = \int_{\Gamma_i} \mathbf{v}^T \mathbf{t}_d d\Gamma \quad (27)$$

Note that the term $(\mathbf{C}_{xx}^T \mathbf{n}) / |\Omega_i|$ formally corresponds to a vector of boundary tractions along the boundary of Ω_i . Therefore, we can interpret $\mathbf{t}_d = (\mathbf{C}_{xx}^T \mathbf{n}) / |\Omega_i|$ as a vector of boundary tractions applied along the boundary of the sub-domain of interest Γ_i , which can be used to extract the mean strain in Ω_i .

For any given linear combination of strains ϵ_η , denoted as

$$\epsilon_\eta = c_{\epsilon_{xx}} \epsilon_{xx} + c_{\epsilon_{yy}} \epsilon_{yy} + c_{\epsilon_{xy}} \epsilon_{xy} = \mathbf{c}_{\epsilon_\eta}^T \boldsymbol{\epsilon} = \nabla \cdot (\mathbf{G} \mathbf{u}) \quad (28)$$

where

$$\mathbf{G} = c_{\epsilon_{xx}} \mathbf{C}_{xx} + c_{\epsilon_{yy}} \mathbf{C}_{yy} + c_{\epsilon_{xy}} \mathbf{C}_{xy} \quad (29)$$

we could evaluate an expression similar to (27) such that

$$Q(\mathbf{v}) = \int_{\Gamma_i} \mathbf{v}^T \left(\frac{\mathbf{G}^T \mathbf{n}}{|\Omega_i|} \right) d\Gamma = \int_{\Gamma_i} \mathbf{v}^T \mathbf{t}_d d\Gamma. \quad (30)$$

4.4 Mean stress value in Ω_i

Let us consider now as QoI the mean stress value $\bar{\sigma}_\alpha|_{\Omega_i}$ given by a combination of the stress components in a domain of interest which reads:

$$Q(\mathbf{u}) = \bar{\sigma}_\alpha|_{\Omega_i} = \frac{1}{|\Omega_i|} \int_{\Omega_i} \sigma_\alpha d\Omega = \frac{1}{|\Omega_i|} \int_{\Omega_i} \mathbf{c}_{\sigma_\alpha}^T \boldsymbol{\sigma} d\Omega. \quad (31)$$

The stress components are linear combinations of the strain components. Thus, any combination of stress components σ_α can be expressed as:

$$\sigma_\alpha = \mathbf{c}_{\sigma_\alpha}^T \boldsymbol{\sigma} = \mathbf{c}_{\sigma_\alpha}^T \mathbf{D} \boldsymbol{\epsilon} = \mathbf{c}_{\epsilon_\eta}^T \boldsymbol{\epsilon}, \quad (32)$$

where $\mathbf{c}_{\sigma_\alpha}$ is the vector used to define the combination of stress components and $\mathbf{c}_{\epsilon_\eta}$ defines its corresponding combination of strain components. Therefore, one could evaluate the mean value of any combination $\mathbf{c}_{\sigma_\alpha}$ of stress components in Ω_i using (30), where \mathbf{G} is evaluated using the coefficients of $\mathbf{c}_{\epsilon_\eta}^T = \mathbf{c}_{\sigma_\alpha}^T \mathbf{D}$ in (29).

4.5 Mean stresses and strains in a domain of interest from the perspective of initial stresses and strains

Previously, the expressions to calculate mean stresses or strains in a domain of interest Ω_i have been obtained using the divergence theorem. However, we can calculate these quantities of interest considering them as an initial stress load case in the dual problem. This can be proved immediately

$$Q(\mathbf{u}) = \bar{\sigma}_\alpha|_{\Omega_i} = \frac{1}{|\Omega_i|} \int_{\Omega_i} \mathbf{c}_{\sigma_\alpha}^T \boldsymbol{\sigma} d\Omega = \int_{\Omega_i} \frac{\mathbf{c}_{\sigma_\alpha}^T}{|\Omega_i|} \boldsymbol{\sigma} d\Omega \quad (33)$$

From (5) we can define $\boldsymbol{\epsilon}_{0,d} = \mathbf{c}_{\sigma_\alpha}^T / |\Omega_i|$ corresponding to the term of initial strains that we need to apply in the dual problem to extract the value of $\bar{\sigma}_\alpha|_{\Omega_i}$. A similar formulation can be derived for the case of the mean strains in Ω_i such that $\boldsymbol{\sigma}_{0,d} = \mathbf{c}_{\epsilon_\eta}^T / |\Omega_i|$.

4.6 Mean tractions along Γ_i

Let $\mathbf{t} = \{t_n, t_t\}^T$, with t_n and t_t the normal and tangential components of the tractions vector \mathbf{t} . Let us assume that we want to evaluate, for example, the mean normal tractions along boundary Γ_i . The functional that defines the mean tractions along the boundary Γ_i can be expressed as

$$Q(\mathbf{u}) = \bar{\mathbf{t}}_n = \frac{1}{|\Gamma_i|} \int_{\Gamma_i} \mathbf{t}^T \mathbf{c} d\Gamma \quad (34)$$

Using (34) and considering the extraction vector \mathbf{c} and the rotation matrix \mathbf{R}_Γ that aligns the tractions normal to the boundary Γ_i we have:

$$\begin{aligned} \bar{\mathbf{t}}_n &= \frac{1}{|\Gamma_i|} \int_{\Gamma_i} \mathbf{t}^T \mathbf{c} d\Gamma \\ &= \frac{1}{|\Gamma_i|} \int_{\Gamma_i} \{t_n \ t_t\} \begin{Bmatrix} 1 \\ 0 \end{Bmatrix} d\Gamma \\ &= \frac{1}{|\Gamma_i|} \int_{\Gamma_i} \{t_x \ t_y\} \mathbf{R}_\Gamma^T \begin{Bmatrix} 1 \\ 0 \end{Bmatrix} d\Gamma \\ &= \int_{\Gamma_i} \{t_x \ t_y\} \frac{\mathbf{R}_\Gamma^T}{|\Gamma_i|} \begin{Bmatrix} 1 \\ 0 \end{Bmatrix} d\Gamma \\ &= \int_{\Gamma_i} \{t_x \ t_y\} \mathbf{u}_d d\Gamma \end{aligned} \quad (35)$$

In (35) the term $\mathbf{u}_d = \mathbf{R}_\Gamma^T \mathbf{c} / |\Gamma_i|$ corresponds to a vector of displacements used as Dirichlet boundary conditions for the dual problem used to extract the mean value of the normal tractions along Γ_i .

Note that in this case $\bar{\mathbf{w}}_Q = \mathbf{u}_d \neq 0$, then (12) does not hold. We redefine the dual problem in (11), $\forall \mathbf{v} \in V$, such that:

$$\begin{aligned} a(\mathbf{v}, \mathbf{w}_Q) &= 0 \quad \text{in } \Omega \\ \mathbf{w}_Q &= \mathbf{u}_d \quad \text{on } \Gamma_i \end{aligned} \quad (36)$$

The dual solution can be expressed as $\mathbf{w}_Q = \mathbf{w}_Q^0 + \bar{\mathbf{w}}_Q$, where $\mathbf{w}_Q^0 = 0$ on Γ_i . Assuming that $\bar{\mathbf{w}}_Q = \mathbf{u}_d$ is in the FE solution space, the FE approximation for (36) is also decomposed into two parts $\mathbf{w}_Q^h = \mathbf{w}_Q^{h0} + \bar{\mathbf{w}}_Q$ where, again, $\mathbf{w}_Q^{h0} = 0$ on Γ_i . Therefore, we have for the dual problem

$$\begin{aligned} \forall \mathbf{v} \in V \quad a(\mathbf{v}, \mathbf{w}_Q) &= a(\mathbf{v}, \mathbf{w}_Q^0) + a(\mathbf{v}, \bar{\mathbf{w}}_Q) = 0 \\ \forall \mathbf{v} \in V \quad a(\mathbf{v}, \mathbf{w}_Q^0) &= -a(\mathbf{v}, \bar{\mathbf{w}}_Q) \end{aligned} \quad (37)$$

Substituting $\mathbf{v} = \mathbf{e}$ in (37), using the Galerkin orthogonality property, $a(\mathbf{e}, \mathbf{w}_Q^{h0}) = 0$, and considering that $\mathbf{e}_Q^0 = \mathbf{e}_Q$ we write:

$$a(\mathbf{e}, \mathbf{w}_Q^0 - \mathbf{w}_Q^{h0}) = a(\mathbf{e}, \mathbf{e}_Q^0) = a(\mathbf{e}, \mathbf{e}_Q) = -a(\mathbf{e}, \bar{\mathbf{w}}_Q) \quad (38)$$

Similarly, the QoI can also be rewritten by means of the divergence theorem. Thus, generalizing (35) $\forall \mathbf{v} \in V$ we have:

$$Q(\mathbf{v}) = \int_{\Gamma_i} (\mathbf{Q}\boldsymbol{\sigma}(\mathbf{v}))^T \mathbf{u}_d \, d\Gamma = \int_{\Omega_i} \boldsymbol{\sigma}(\mathbf{v})^T \boldsymbol{\epsilon}(\mathbf{u}_d) \, d\Omega = a(\mathbf{v}, \mathbf{u}_d) \quad (39)$$

where \mathbf{Q} is the matrix form of the Cauchy's law considering the unit normal vector to Γ_i , such that $\mathbf{t}_{\Gamma_i} = \mathbf{Q}\boldsymbol{\sigma}$. Thus, $Q(\mathbf{e}) = a(\mathbf{e}, \mathbf{u}_d) = a(\mathbf{e}, \bar{\mathbf{w}}_Q)$ and substituting in (38) we obtain the error for this QoI: $Q(\mathbf{e}) = -a(\mathbf{e}, \mathbf{e}_Q)$.

4.7 Generalised stress intensity factor in Ω_i

Consider the problem of evaluating the generalised stress intensity factor (GSIF), that characterises the singular solution in problems with reentrant corners and cracks, as the quantity of interest.

From [33, 34] we take the expression to evaluate the GSIF, which reads:

$$Q(\mathbf{u}) = K^{(1,2)} = -\frac{1}{C} \int_{\Omega_i} \left(\sigma_{jk}^{(1)} u_k^{(2)} - \sigma_{jk}^{(2)} u_k^{(1)} \right) \frac{\partial q}{\partial x_j} \, d\Omega \quad (40)$$

where $u^{(1)}, \sigma^{(1)}$ are the displacement and stress fields from the FE solution, $u^{(2)}, \sigma^{(2)}$ are the auxiliary fields used to extract the GSIFs in mode I or mode II and C is a constant that is dependent on the geometry and the loading mode. q is an arbitrary C^0 function used to define the extraction zone which must take the value of 1 at the singular point and 0 at the boundaries and x_j refers to the local coordinate system defined at the singularity.

Rearranging terms in the integral in (40) we obtain:

$$Q(\mathbf{u}) = K^{(1,2)} = \int_{\Omega_i} (\boldsymbol{\sigma}^{(1)})^T \left(-\frac{1}{C} \right) \begin{bmatrix} u_1^{(2)} q_{,1} \\ u_2^{(2)} q_{,2} \\ u_2^{(2)} q_{,1} + u_1^{(2)} q_{,2} \end{bmatrix} - (\mathbf{u}^{(1)})^T \left(-\frac{1}{C} \right) \begin{bmatrix} \sigma_{11}^{(2)} q_{,1} + \sigma_{21}^{(2)} q_{,2} \\ \sigma_{12}^{(2)} q_{,1} + \sigma_{22}^{(2)} q_{,2} \end{bmatrix} \, d\Omega \quad (41)$$

which could be rewritten as a function of initial strains $\boldsymbol{\epsilon}_0$ and body loads \mathbf{b} :

$$Q(\mathbf{u}) = K^{(1,2)} = \int_{\Omega_i} (\boldsymbol{\sigma}^{(1)}(\mathbf{u}))^T \boldsymbol{\epsilon}_0 + (\mathbf{u}^{(1)})^T \mathbf{b} \, d\Omega \quad (42)$$

Thus, if we replace \mathbf{u} with the vector of arbitrary displacements \mathbf{v} , the quantity of interest can be evaluated from

$$Q(\mathbf{v}) = \int_{\Omega_i} \mathbf{L} \mathbf{v}^T \mathbf{D} \boldsymbol{\epsilon}_{0,d} \, d\Omega + \int_{\Omega_i} \mathbf{v}^T \mathbf{b}_d \, d\Omega. \quad (43)$$

Hence, the initial strains and the body loads per unit volume that must be applied in the dual problem to extract the GSIF are defined as

$$\boldsymbol{\epsilon}_{0,d} = -\frac{1}{C} \begin{bmatrix} u_1^{(2)} q_{,1} \\ u_2^{(2)} q_{,2} \\ u_2^{(2)} q_{,1} + u_1^{(2)} q_{,2} \end{bmatrix}, \quad \mathbf{b}_d = \frac{1}{C} \begin{bmatrix} \sigma_{11}^{(2)} q_{,1} + \sigma_{21}^{(2)} q_{,2} \\ \sigma_{12}^{(2)} q_{,1} + \sigma_{22}^{(2)} q_{,2} \end{bmatrix} \quad (44)$$

5 Recovery technique

As noted in previous sections, a widely used technique to control the error in the energy norm in the finite element discretization is the Zienkiewicz-Zhu error estimator shown in (9), which is based on the recovery of an enhanced stress field $\boldsymbol{\sigma}^*$. The accuracy of such estimates depends on the quality of the recovered field. To improve the quality of the recovered fields, numerical results indicate that when recovering singular fields, statical admissibility and suitably chosen enrichment functions improve the accuracy [18, 35]². In this work we consider the SPR-CX recovery technique, which is an enhancement of the error estimator introduced in [26], to recover the solutions for both the primal and dual problems. The technique incorporates the ideas in [12] to guarantee locally on patches the exact satisfaction of the equilibrium equations, and the extension in [15] to singular problems.

In the SPR-CX technique, as in the original SPR technique, a patch is defined as the set of elements connected to a vertex node. On each patch, a polynomial expansion for each one of the components of the recovered stress field is expressed in the form:

$$\sigma_k^*(\mathbf{x}) = \mathbf{p}(\mathbf{x})\mathbf{a}_k \quad k = xx, yy, xy \quad (45)$$

where \mathbf{p} represents a polynomial basis and \mathbf{a} are unknown coefficients. Usually, the polynomial basis is chosen equal to the finite element basis for the displacements.

For the 2D case, the linear system of equations to evaluate the recovered stress field coupling the three stress components reads:

$$\boldsymbol{\sigma}^*(\mathbf{x}) = \begin{Bmatrix} \sigma_{xx}^*(\mathbf{x}) \\ \sigma_{yy}^*(\mathbf{x}) \\ \sigma_{xy}^*(\mathbf{x}) \end{Bmatrix} = \mathbf{P}(\mathbf{x})\mathbf{A} = \begin{bmatrix} \mathbf{p}(\mathbf{x}) & \mathbf{0} & \mathbf{0} \\ \mathbf{0} & \mathbf{p}(\mathbf{x}) & \mathbf{0} \\ \mathbf{0} & \mathbf{0} & \mathbf{p}(\mathbf{x}) \end{bmatrix} \begin{Bmatrix} \mathbf{a}_{xx} \\ \mathbf{a}_{yy} \\ \mathbf{a}_{xy} \end{Bmatrix} \quad (46)$$

Constraint equations are introduced via Lagrange multipliers into the linear system used to solve for the coefficients \mathbf{A} on each patch in order to enforce the satisfaction of the:

- Internal equilibrium equations.
- Boundary equilibrium equations: A point collocation approach is used to impose the satisfaction of a polynomial approximation to the tractions along the Neumann boundary intersecting the patch.
- Compatibility equations: This additional constraint is also imposed to further increase the accuracy of the recovered stress field.

Different techniques have been proposed to account for the singular part during the recovery process [15, 13, 16]. Here, following the ideas in [15], for singular

²The use of enrichment to improve recovery based error estimates for enriched approximations was discussed in detail in some of the first papers discussing derivative recovery techniques for enriched finite element approximations, see References [13, 14, 16]. A very detailed and clear discussion of a wide variety of error estimators and adaptive procedures for discontinuous failure is provided in [36].

problems the exact stress field $\boldsymbol{\sigma}$ is decomposed into two stress fields, a smooth field $\boldsymbol{\sigma}_{\text{smo}}$ and a singular field $\boldsymbol{\sigma}_{\text{sing}}$:

$$\boldsymbol{\sigma} = \boldsymbol{\sigma}_{\text{smo}} + \boldsymbol{\sigma}_{\text{sing}}. \quad (47)$$

Then, the recovered field $\boldsymbol{\sigma}^*$ required to compute the error estimate given in (9) can be expressed as the contribution of two recovered stress fields, one smooth $\boldsymbol{\sigma}_{\text{smo}}^*$ and one singular $\boldsymbol{\sigma}_{\text{sing}}^*$:

$$\boldsymbol{\sigma}^* = \boldsymbol{\sigma}_{\text{smo}}^* + \boldsymbol{\sigma}_{\text{sing}}^*. \quad (48)$$

For the recovery of the singular part, the expressions which describe the asymptotic fields near the crack tip are used. To evaluate $\boldsymbol{\sigma}_{\text{sing}}^*$ we first obtain estimated values of the stress intensity factors K_I and K_{II} using a domain integral method based on extraction functions [33, 37]. Notice that the recovered part $\boldsymbol{\sigma}_{\text{sing}}^*$ is an equilibrated field as it satisfies the equilibrium equations.

Once the field $\boldsymbol{\sigma}_{\text{sing}}^*$ has been evaluated, an FE-type (discontinuous) approximation to the smooth part $\boldsymbol{\sigma}_{\text{smo}}^h$ can be obtained subtracting $\boldsymbol{\sigma}_{\text{sing}}^*$ from the raw FE field:

$$\boldsymbol{\sigma}_{\text{smo}}^h = \boldsymbol{\sigma}^h - \boldsymbol{\sigma}_{\text{sing}}^*. \quad (49)$$

Then, the field $\boldsymbol{\sigma}_{\text{smo}}^*$ is evaluated applying the enhancements of the SPR technique previously described, i.e. satisfaction of equilibrium and compatibility equations in each patch. Note that as both $\boldsymbol{\sigma}_{\text{smo}}^*$ and $\boldsymbol{\sigma}_{\text{sing}}^*$ satisfy the equilibrium equations, $\boldsymbol{\sigma}^*$ also satisfies equilibrium on each patch. A similar approach is followed in the case where an initial stress or strain is applied. We subtract the *a priori* known information ($\boldsymbol{\sigma}_0$ or $\boldsymbol{\epsilon}_0$) from the FE stress field, then we perform the recovery and finally add again $\boldsymbol{\sigma}_0$ or $\boldsymbol{\epsilon}_0$.

To obtain a continuous field, the recovered stresses $\boldsymbol{\sigma}^*$ are directly evaluated at an integration point \mathbf{x} through a partition of unity procedure [29], properly weighting the stress interpolation polynomials obtained from the different patches formed at the vertex nodes of the element containing \mathbf{x} :

$$\boldsymbol{\sigma}^*(\mathbf{x}) = \sum_{J=1}^{n_v} N_J(\mathbf{x}) \boldsymbol{\sigma}_J^*(\mathbf{x}_J), \quad (50)$$

where N_J are the shape functions associated with the vertex nodes n_v . However, this process introduces a lack of equilibrium $\mathbf{s} = \sum_{J=1}^{n_v} \nabla N_J \cdot \boldsymbol{\sigma}_J^*$ when evaluating the divergence of the internal equilibrium equation, as explained in [26, 27].

This recovery technique, used to obtain the recovered field for the primal problem $\boldsymbol{\sigma}_p^*$, is also used to evaluate $\boldsymbol{\sigma}_d^*$ considering different loading conditions. Two remarks are worth being made here. First, the analytical expressions that define the tractions \mathbf{t} and body forces \mathbf{b} for the dual problem are obtained from the interpretation of the functional $Q(\mathbf{u})$ in terms of \mathbf{t}_d and \mathbf{b}_d , as seen in Section 4. Second, to enforce equilibrium conditions along the boundary of the domain of interest (DoI), we consider a different polynomial expansion on each side of the boundary and enforce statical admissibility of the normal and tangential stresses. Suppose that we have a patch intersected by Γ_i such that $\Omega_e = \Omega_{1,e} \cup \Omega_{2,e}$ for intersected elements, as indicated in Figure 1. To enforce equilibrium conditions along Γ_i we define the

stresses $\sigma_{\Omega_1}^*|_{\Gamma_i}$, $\sigma_{\Omega_2}^*|_{\Gamma_i}$ on each side of the internal boundary. Then, the boundary equilibrium along Γ_i is:

$$\mathbf{Q}(\sigma_{\Omega_1}^*|_{\Gamma_i} - \sigma_{\Omega_2}^*|_{\Gamma_i}) = \mathbf{t}_{\Gamma_i} \quad (51)$$

where $\mathbf{t}_{\Gamma_i} = [t_x \ t_y]^T$ are the prescribed tractions, e.g. those obtained from (27), and \mathbf{Q} is the matrix form of Cauchy's law considering the unit normal \mathbf{n} to Γ_i such that

$$\mathbf{Q} = \begin{bmatrix} n_x & 0 & n_y \\ 0 & n_y & n_x \end{bmatrix} \quad (52)$$

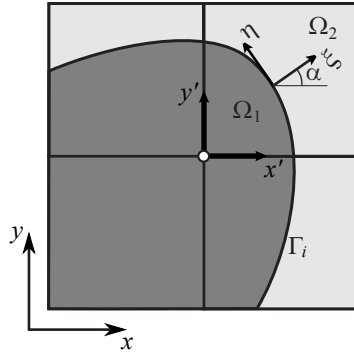


Figure 1: Equilibrium conditions along internal boundaries.

6 Numerical results

In this section numerical tests using 2D benchmark problems with exact solutions are used to investigate the quality of the proposed technique. The first problem has a smooth solution whilst the second is a singular problem. For both models we assume plane strain conditions. The h -adaptive FE code used in the numerical examples is based on Cartesian meshes independent of the problem geometry [38], with linear quadrilateral (Q4) elements³. To represent the domain geometry accurately, the integrals in elements cut by the boundary are restricted to the part of the element within the domain as in [40, 41]. The integration procedure in these elements is based on the definition of triangular integration subdomains within Ω_e and aligning with the geometry of the domain. In elements cut by curved boundaries, these triangular subdomains can have curved boundaries. In that case, the actual geometry is reproduced using a transfinite mapping [42, 43]. Dirichlet boundary conditions are imposed using Lagrange multipliers following a procedure similar to that described in [44] and, more recently [39]. In cases where the geometry boundary cuts the mesh close to a node, preconditioning techniques are necessary, and the authors recommend the simple domain decomposition approach of [45]⁴.

³The interested reader is referred to the recent paper by Moumnassi and colleagues [39] which discusses recent advances in “ambient space finite elements” and proposes hybrid level set/FEMs able to handle sharp corners and edges.

⁴The interested reader may want to refer to the most insightful papers of [46] and [47, 48], the latter two being based on algebraic multi grid approaches.

To assess the performance of the proposed technique we consider the effectivity index of the error estimator θ defined as the quotient of estimated error $Q(\mathbf{e}_{es})$ in the quantity of interest over the exact error $Q(\mathbf{e})$:

$$\theta = \frac{Q(\mathbf{e}_{es})}{Q(\mathbf{e})}, \quad (53)$$

We can also represent the effectivity in the QoI θ_{QoI} , defined as the corrected value of the QoI $Q(\mathbf{u}^h)$ using the error estimate, divided by the exact value $Q(\mathbf{u})$:

$$\theta_{QoI} = \frac{Q(\mathbf{u}^h) + Q(\mathbf{e}_{es})}{Q(\mathbf{u})}. \quad (54)$$

The relative error in the QoI for the exact and estimated error are

$$\eta^Q(\mathbf{e}) = \frac{|Q(\mathbf{e})|}{|Q(\mathbf{u})|}, \quad \eta^Q(\mathbf{e}_{es}) = \frac{|Q(\mathbf{e}_{es})|}{|Q(\mathbf{u}^h) + Q(\mathbf{e}_{es})|}. \quad (55)$$

The distribution of the local effectivity index D is analysed at element level, following the definitions described in [12] for the error in energy norm, adapted here to the case of the error in QoI:

$$\begin{aligned} D &= \theta^e - 1 & \text{if } \theta^e \geq 1 \\ D &= 1 - \frac{1}{\theta^e} & \text{if } \theta^e < 1 \end{aligned} \quad \text{with} \quad \theta^e = \frac{Q(\mathbf{e}_{es}^e)}{Q(\mathbf{e}^e)} \quad (56)$$

where superscript e denotes evaluation at element level. To evaluate $Q(\mathbf{e}^e)$ and $Q(\mathbf{e}_{es}^e)$ we use (13, 17) locally in each element. Nonetheless, we should remark that this is only possible for some problems with analytical solutions as the exact value of σ is unknown in the vast majority of cases, especially for the dual problem.

Once error in the QoI has been estimated, the local error estimates in each element can be used to perform h -adaptive analyses using similar techniques to those already available for the error in the energy norm. The refinement of the mesh using the error estimate as the guiding parameter considers an stopping criterion that checks the value of the estimated error against a prescribed or desired error. If the estimated error is higher than the desired error then the mesh is refined. Several procedures to perform the refinement are available in the literature. To define the size of the elements in the new mesh we follow the adaptive process described in [49, 50, 51] which minimises the number of elements in the new mesh for a given accuracy level. This criterion is equivalent to the traditional approach of equally distributing the error in each element of the new mesh as shown in [52, 53]. These criteria provide the size of the elements in the new mesh as a function of i) the ratio of the estimated error in energy norm in the current mesh to the desired error in the new mesh, and ii) the estimated error in energy norm in each element, which always take non negative values. They cannot be directly used in goal-oriented adaptivity because the local contributions to the global error in the QoI, evaluated in each element using (17), can take negative values. Thus, for our implementation using h -adaptive routines developed for the error in energy norm we prepare as input the square root of the absolute value of the error in the QoI – following the relation

from the expressions in (8, 13) – and the ratio of the estimated error in the QoI in the current mesh to the desired error in the new mesh.

The refinement technique provides a distribution of the required new element sizes. These sizes are specified in each element of the current mesh, which will be recursively split into 4 new elements until the sizes of the elements are smaller than the required size. A maximum difference of only one refinement level will be allowed between adjacent elements. In these cases C^0 continuity will be enforced by means of the use of multipoint constraints [54, 55].

6.1 Problem 1: Thick-wall cylinder subjected to internal pressure.

The geometrical model for this problem and the initial mesh are represented in Figure 2. Due to symmetry, only 1/4 of the section is modelled. The domain of interest (DoI) Ω_i is denoted by a dark square whereas the contours of interest Γ_i and Γ_o are the internal and external surfaces of radius a and b . Young's modulus is $E = 1000$, Poisson's ratio is $\nu = 0.3$, $a = 5$, $b = 20$ and the load $P = 1$.

The exact solution for the radial displacement assuming plane strain conditions is given by

$$u_r(r) = \frac{P(1+\nu)}{E(c^2-1)} \left(r(1-2\nu) + \frac{b^2}{r} \right) \quad (57)$$

where $c = b/a$, $r = \sqrt{x^2 + y^2}$ and $\phi = \arctan(y/x)$. Stresses in cylindrical coordinates are

$$\sigma_r(r) = \frac{P}{c^2-1} \left(1 - \frac{b^2}{r^2} \right) \quad \sigma_\theta(r) = \frac{P}{c^2-1} \left(1 + \frac{b^2}{r^2} \right) \quad \sigma_z(r, \theta) = 2\nu \frac{P}{c^2-1} \quad (58)$$

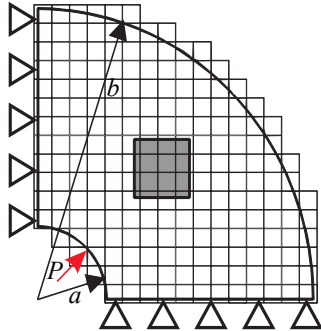


Figure 2: Thick-wall cylinder subjected to an internal pressure. Model and analytical solution, the domain of interest Ω_i is indicated in dark.

Several linear quantities of interest have been considered for this problem: the mean radial displacements along Γ_o , the mean displacements u_x in the domain of interest Ω_i , the mean stresses σ_x in Ω_i and the mean value of the normal tractions along Γ_i . For the last case, instead of applying pressure P , we impose displacements $u_r(a)$ on this surface, see (57).

6.1.1 Problem 1.a.: Mean radial displacements along Γ_o

Let $Q(\mathbf{u})$ be the functional that evaluates the mean normal displacement \bar{u}_n along Γ_o such that:

$$Q(\mathbf{u}) = \bar{u}_n = \frac{1}{|\Gamma_o|} \int_{\Gamma_o} (\mathbf{R}\mathbf{u})^T \mathbf{c}_u d\Gamma \quad (59)$$

where \mathbf{R} is the standard rotation matrix for the displacements that aligns the coordinate system with the boundary Γ_o and $\mathbf{c}_u = \{1, 0\}^T$ is the extraction vector that selects the normal component. Thus, the exact value of the QoI given by (57) for $r = b$ is $\bar{u}_n = 2.426 \cdot 10^{-3}$.

Figure 3 shows the set of meshes resulting from the h -adaptive process guided by the error estimate in this QoI.

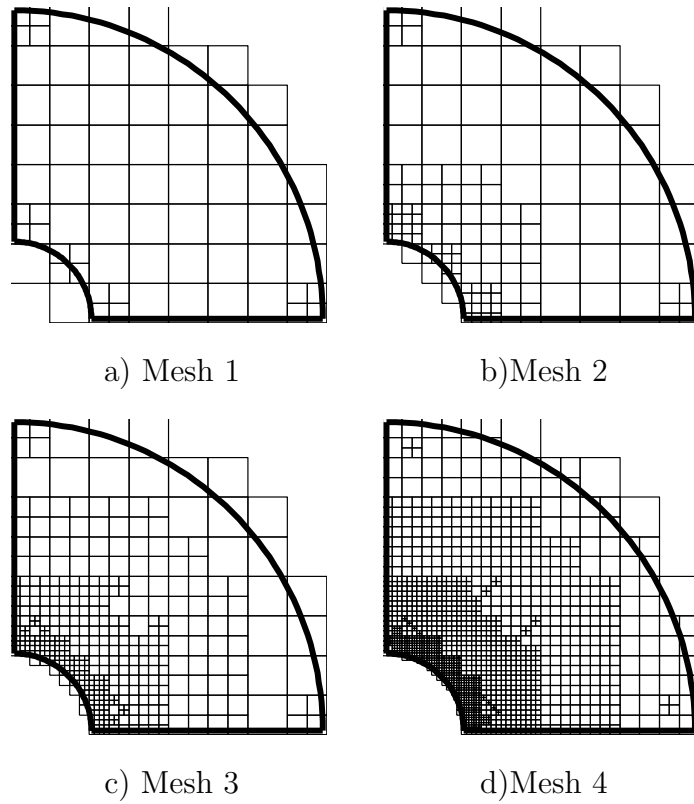


Figure 3: Problem 1.a. Sequence of meshes for the mean displacement in a domain of interest Γ_o .

In Table 1 we show the results for the error estimate $\mathcal{E}_{\text{SPR-CX}} = \mathcal{E}_1$ from (18), evaluated using the SPR-CX recovery technique both in the primal and the dual problems, and the exact error $Q(\mathbf{e})$. The recovery technique accurately captures the exact error and provides good effectivities, with values of $\theta = 0.9473$ for the coarsest mesh with 180 degrees of freedom (dof). The evolution of the effectivity index for the proposed technique and the standard SPR is represented in Figure 4. In this case, SPR-CX converges faster to the optimal value $\theta = 1$ and shows a high level of accuracy ($\theta = 0.9928$ for 3294 dof).

Table 1: Problem 1.a. The table shows the values for the error estimate $\mathcal{E}_{\text{SPR-CX}}$ and effectivities.

dof	$Q(\mathbf{e}_{es}) = \mathcal{E}_{\text{SPR-CX}}$	$Q(\mathbf{e})$	θ	θ_{QoI}
180	$5.909651 \cdot 10^{-5}$	$6.238291 \cdot 10^{-5}$	0.94731888	0.99864571
322	$1.739913 \cdot 10^{-5}$	$1.755027 \cdot 10^{-5}$	0.99138817	0.99993772
937	$4.397256 \cdot 10^{-6}$	$4.459314 \cdot 10^{-6}$	0.98608343	0.99997443
3,294	$1.077612 \cdot 10^{-6}$	$1.085411 \cdot 10^{-6}$	0.99281470	0.99999679

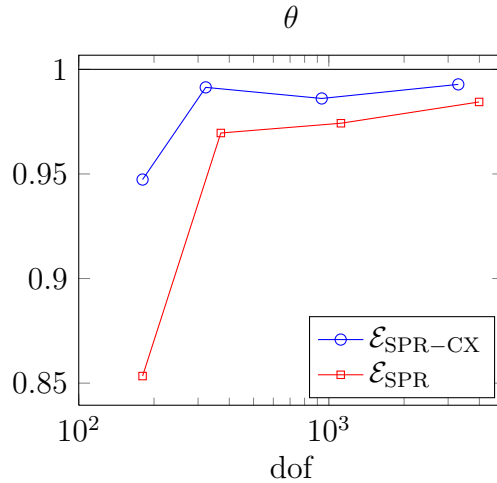


Figure 4: Problem 1.a. Evolution of the effectivity index θ considering locally equilibrated, $\mathcal{E}_{\text{SPR-CX}}$, and non-equilibrated recovery, \mathcal{E}_{SPR} .

Note that in this case, the dual problem corresponds to a traction $\mathbf{t} = \mathbf{R}^T \mathbf{c} / |\Gamma_o|$ that represents a constant traction normal to the external boundary. Therefore, the solution to the dual problem can be evaluated exactly for this quantity of interest using the analytical solution for a cylinder under external pressure:

$$\sigma_r(r) = -\frac{P_o b^2}{b^2 - a^2} \left(1 - \frac{a^2}{r^2}\right) \quad \sigma_\theta(r) = -\frac{P_o b^2}{b^2 - a^2} \left(1 + \frac{a^2}{r^2}\right) \quad (60)$$

where P_o represents the applied external pressure. As the exact solution for the dual problem is available, it is possible to evaluate the local effectivity D in (56) at element level to evaluate the local quality of the error estimate in the quantity of interest. Figure 5 shows the evolution of the mean absolute value $m(|D|)$ and standard deviation $\sigma(D)$ of the local effectivity. The ideal scenario is that both parameters are as small as possible and go to zero as we increase the number of DOFs. In the figure we see that the SPR-CX gives a better local estimation, with values of $\sigma(D)$ and $m(|D|)$ that are smaller than those for the SPR – for the mesh with approx. 3300 dof $\sigma(D) = 0.11$ for the SPR-CX, compared to $\sigma(D) = 0.36$ for the SPR.

As the h -adaptive procedures use local information to refine the mesh, providing an accurate local error estimate to the adaptive algorithm is of critical importance. For this reason, the local performance of the proposed technique indicates that

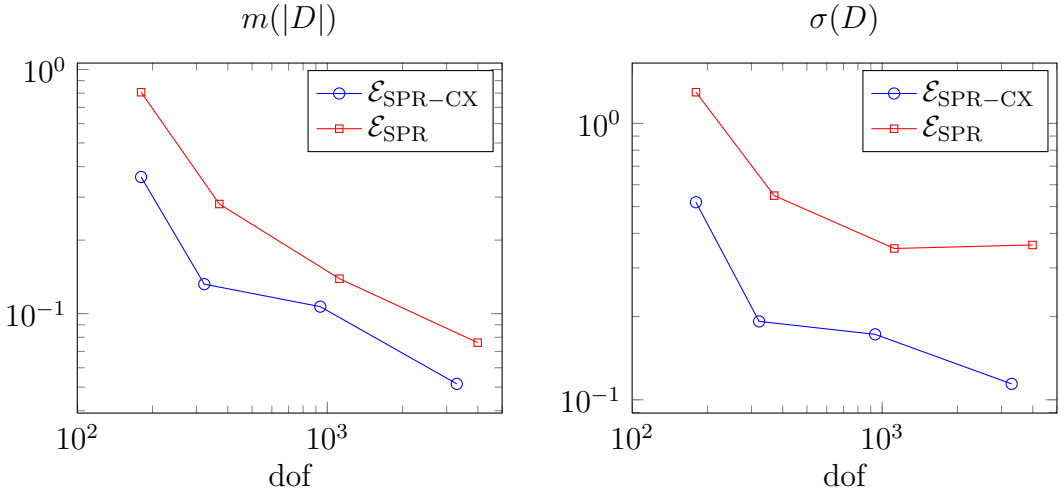


Figure 5: Problem 1.a. Evolution of the mean absolute value $m(|D|)$ and standard deviation $\sigma(D)$ of the local effectivity considering locally equilibrated , $\mathcal{E}_{\text{SPR-CX}}$, and non-equilibrated recovery, \mathcal{E}_{SPR} .

the error estimator based on equilibrated recovered fields for the primal and dual problems is superior to the standard recovery techniques to guide the h -adaptive process, even in cases in which the global effectivity is similar to the effectivity of the standard SPR.

6.1.2 Problem 1.b.: Mean normal traction \bar{t}_n along Γ_i

Consider as quantity of interest the mean normal traction along the inner boundary of the cylinder in Figure 2. As previously mentioned, we consider an equivalent model where displacements are imposed along the inner boundary. The radial displacements to impose are evaluated from (57) such that they correspond to an internal pressure of $P = 1$. In this case, given the displacements we are interested in evaluating the tractions as QoI.

To formulate the dual problem we consider displacement constraints along Γ_i such that

$$u_r(r = a) = \frac{1}{|\Gamma_i|} \quad (61)$$

Table 2 shows the results for the error estimate $\mathcal{E}_{\text{SPR-CX}}$ using the proposed recovery technique and the exact error $Q(\mathbf{e})$. The procedure accurately captures the error and yields good effectivities for this QoI, with values of $\theta = 0.9109$ for the last mesh with 2218 dof. Figure 6 shows the evolution of the effectivity with the number of dof for the SPR-CX and the SPR. Results show a better performance of the proposed technique when compared with the SPR which presents an oscillatory behaviour ($\theta = 0.9466$ for mesh 2 with 260 dof and $\theta = 0.5681$ for mesh 3 with 732 dof).

Figure 7 represents the evolution of the mean absolute value $m(|D|)$ and standard deviation $\sigma(D)$ of the local effectivity. Again, for this example, the SPR-CX gives lower values of these parameters than the SPR. The improved local performance of the SPR-CX is particularly useful for the adaptive algorithm. Notice that for the

Table 2: Problem 1.b. The table shows the values for the error estimate $\mathcal{E}_{\text{SPR-CX}}$ and effectivities.

dof	$Q(\mathbf{e}_{es}) = \mathcal{E}_{\text{SPR-CX}}$	$-Q(\mathbf{e})$	θ	θ_{QoI}
164	$2.245490 \cdot 10^{-1}$	$4.242762 \cdot 10^{-1}$	0.52925199	1.64734771
256	$1.794064 \cdot 10^{-2}$	$2.078322 \cdot 10^{-2}$	0.86322691	1.03855364
652	$3.910983 \cdot 10^{-3}$	$4.170597 \cdot 10^{-3}$	0.93775134	1.00808981
2,218	$1.008523 \cdot 10^{-3}$	$1.107166 \cdot 10^{-3}$	0.91090543	1.00211542

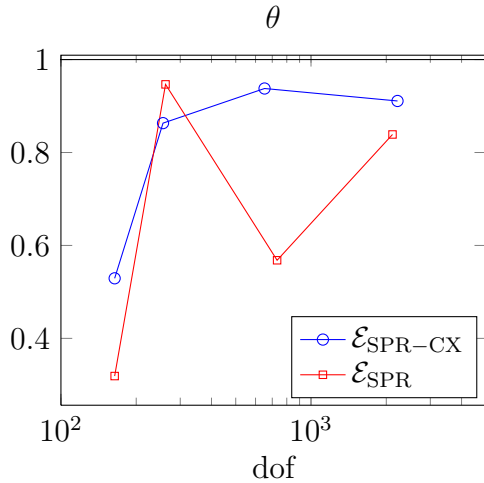


Figure 6: Problem 1.b. Evolution of the effectivity index θ considering locally equilibrated, $\mathcal{E}_{\text{SPR-CX}}$, and non-equilibrated recovery, \mathcal{E}_{SPR} .

second mesh, although the global effectivity is close to unity for the SPR, $m(|D|)$ and $\sigma(D)$ indicate that the SPR-CX is a superior choice when estimating the true error at the element level. Thus, the apparent satisfactory behaviour of the SPR in mesh 2 is due to error compensations of large values of local effectivities.

6.1.3 Problem 1.c.: Mean displacements \bar{u}_x in Ω_i

Let us consider the mean displacement \bar{u}_x in Ω_i as the quantity of interest. The objective is to evaluate the error when evaluating \bar{u}_x defined by the functional:

$$Q(\mathbf{u}) = \bar{u}_x = \frac{1}{|\Omega_i|} \int_{\Omega_i} u_x d\Omega \quad (62)$$

The exact value of the QoI can be computed for this problem and is $\bar{u}_x = 0.002238239291713$. Figure 8 shows the first four meshes used in the h -adaptive refinement process guided by the error estimate for the QoI.

Figure 9 shows the relative error (in percentage) for the error estimates in (18) evaluated using the proposed recovery technique. The exact error $Q(\mathbf{e})$ is also represented for comparison. For all the curves the relative error decreases monotonically when increasing the number of dof, indicating that the h -adaptive process has a stable convergence. The most accurate estimation is obtained for the estimate \mathcal{E}_1 ,

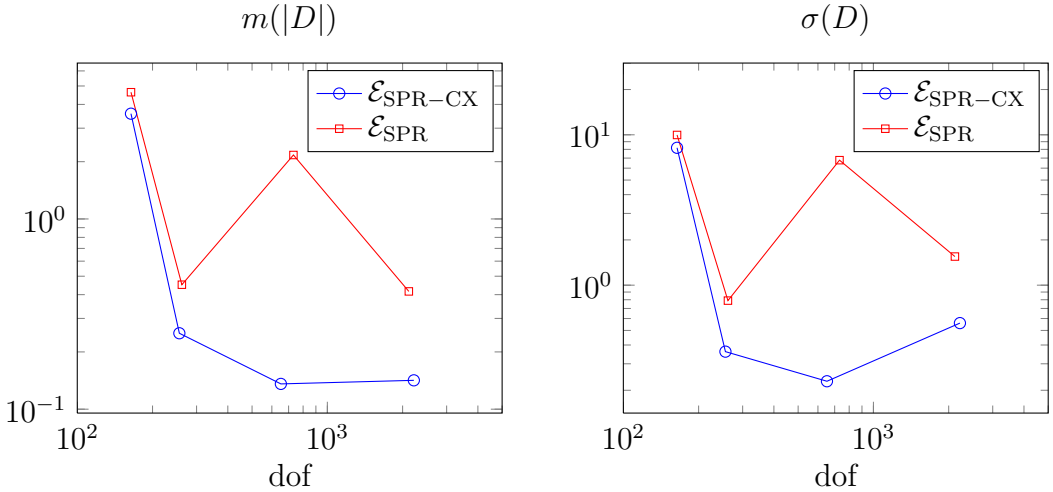


Figure 7: Problem 1.b. Evolution of the mean absolute value $m(|D|)$ and standard deviation $\sigma(D)$ of the local effectivity considering locally equilibrated , $\mathcal{E}_{\text{SPR-CX}}$, and non-equilibrated recovery, \mathcal{E}_{SPR} .

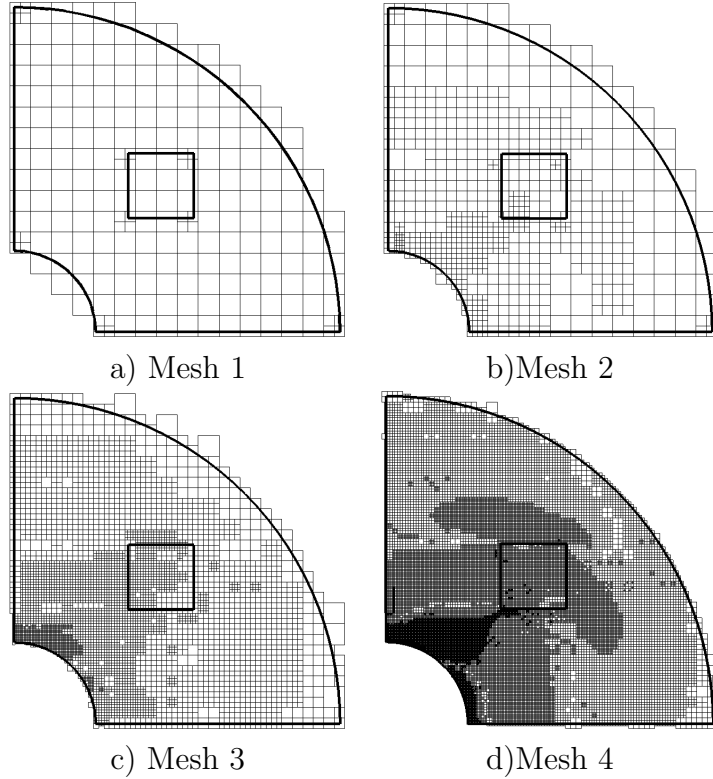


Figure 8: Problem 1.c. Sequence of h -adaptive refined meshes.

which practically coincides with the exact relative error. The other estimates tend to overestimate the exact error, although strictly speaking they do not have bounding properties, which is in agreement with the observations made previously in Section 3.2. Figure 10 represents the evolution of the effectivity index as we increase the number of dof. The curves are in consonance with the results in Figure 9 and show good values for the effectivity index, especially for \mathcal{E}_1 with values between

$[0.9898, 1.0481]$.

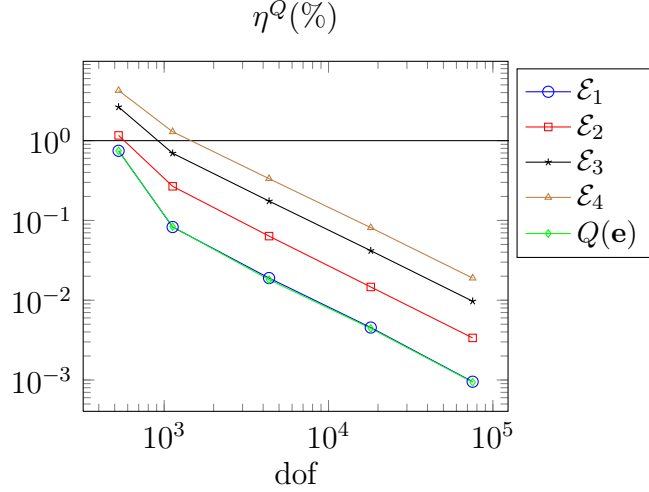


Figure 9: Problem 1.c. Evolution of the relative error η^Q considering the error estimates in (18) and the exact error $Q(\mathbf{e})$.

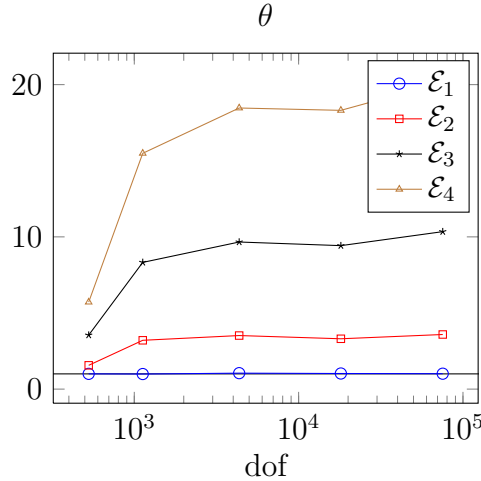


Figure 10: Problem 1.c. Evolution of the effectivity index θ for the error estimates in (18)

Table 3 shows the estimated error in the QoI $Q(\mathbf{e}_{es})$, the exact error $Q(\mathbf{e})$, the effectivity in the quantity of interest θ_{QoI} and the effectivity of the error estimator θ for the sharp error estimate $\mathcal{E}_{SPR-CX} = \mathcal{E}_1$. Comparing $Q(\mathbf{e})$ and $Q(\mathbf{e}_{es})$ we can notice that both values decrease as we refine and that the estimate \mathcal{E}_{SPR-CX} gives a good approximation of the exact error. The effectivity of the error estimator θ converges and is very close to the theoretical value $\theta = 1$ (with $\theta = 1.0123$ for 75323 dof). As expected from these results, the effectivity θ_{QoI} is very accurate as well, with $\theta_{QoI} = 1.00000012$ for 75323 dof.

If in (18a) we consider the case of the non-equilibrated superconvergent patch recovery procedure, resembling the averaging error estimators presented in [24], we

Table 3: Problem 1.c. Error estimate $\mathcal{E}_{\text{SPR-CX}}$ and its effectivities.

dof	$Q(\mathbf{e}_{es}) = \mathcal{E}_{\text{SPR-CX}}$	$Q(\mathbf{e})$	θ	θ_{QoI}
528	$1.670429 \cdot 10^{-5}$	$1.666535 \cdot 10^{-5}$	1.00233710	1.00001740
1,126	$1.849599 \cdot 10^{-6}$	$1.868635 \cdot 10^{-6}$	0.98981317	0.99999150
4,348	$4.240859 \cdot 10^{-7}$	$4.046075 \cdot 10^{-7}$	1.04814162	1.000000870
18,076	$1.017070 \cdot 10^{-7}$	$9.922496 \cdot 10^{-8}$	1.02501376	1.000000111
75,328	$2.128196 \cdot 10^{-8}$	$2.102331 \cdot 10^{-8}$	1.01230285	1.000000012

obtain the results shown in Figure 11. This figure shows that, in this case, the effectivity of the error estimator provided by the standard SPR technique is similar to the effectivity obtained with the SPR-CX technique here proposed, although the latter results in more accurate values for the coarsest mesh ($\theta = 1.1659$ for the SPR and $\theta = 1.0023$ for the SPR-CX, considering 528 dof). In any case, we should recall that the local behaviour with the SPR-CX tends to be better than with the SPR.

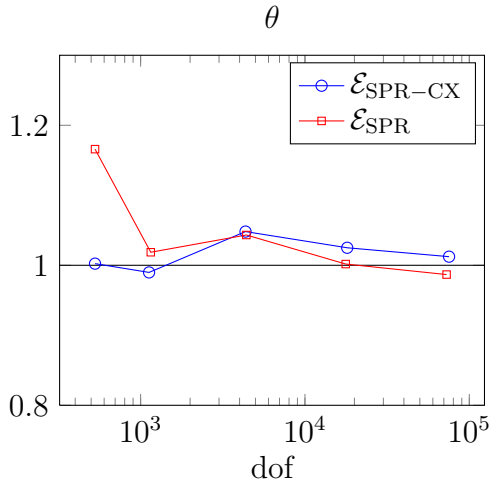


Figure 11: Problem 1.c. Evolution of the effectivity index θ considering equilibrated $\mathcal{E}_{\text{SPR-CX}}$ and non-equilibrated recovery, \mathcal{E}_{SPR} .

6.1.4 Problem 1.d.: Mean stress $\bar{\sigma}_x$ in Ω_i

Consider as QoI the mean stress value $\bar{\sigma}_x$ given in (31). Figure 12 shows the first four meshes of bilinear elements used in the refinement process guided by the error estimated for this QoI.

The evolution of the relative error for the estimates presented in (18) using the proposed recovery technique and the exact error is shown in Figure 13. Similar to the observations done for the previous examples, the most accurate results are obtained when considering the estimate \mathcal{E}_1 . In this case, the other estimates considerably overestimate the true error. Figure 14 shows the effectivity index for $\mathcal{E}_{\text{SPR-CX}}$, which uses the locally equilibrated SPR-CX recovery technique, together with the effectivity obtained with the non-equilibrated SPR technique (\mathcal{E}_{SPR} curve). This

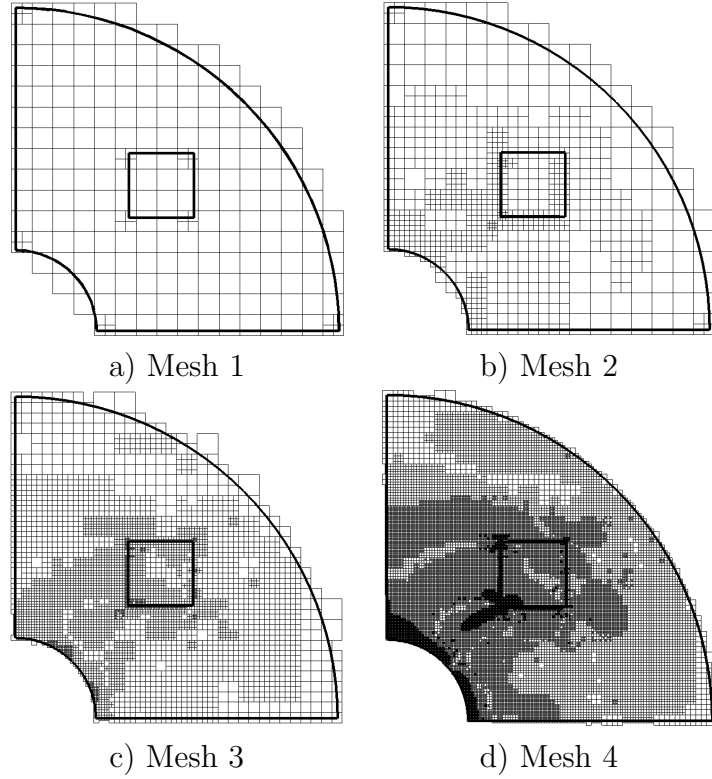


Figure 12: Problem 1.d. Sequence of meshes for the mean stress in a domain of interest.

graph clearly shows the improvement obtained with the SPR-CX recovery technique, with effectivities very close to 1 ($\theta = 0.9797$ for the SPR-CX whilst $\theta = 1.6209$ for the SPR, considering 19573 dof), in contrast with the unstable behaviour of the SPR technique.

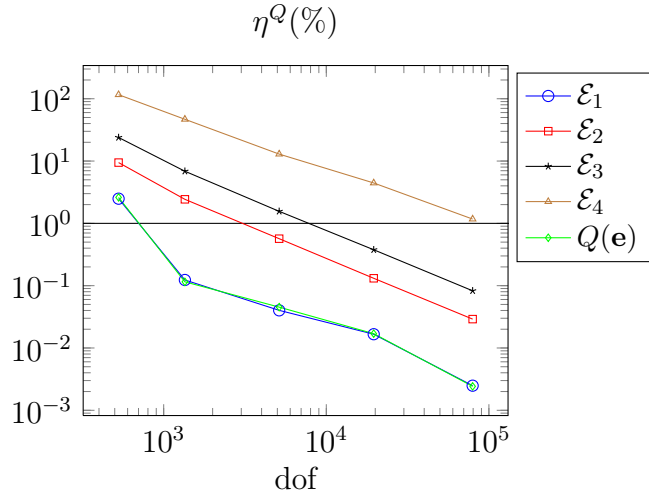


Figure 13: Problem 1.d. Evolution of the relative error η^Q considering the error estimates in (18) and the exact error $Q(\mathbf{e})$.

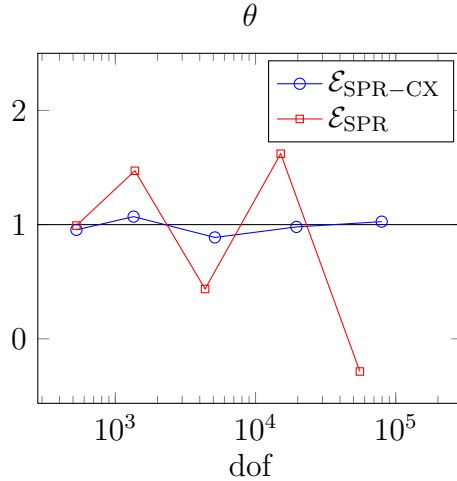


Figure 14: Problem 1.d. Evolution of the effectivity index θ considering equilibrated, $\mathcal{E}_{\text{SPR-CX}}$, and non-equilibrated recovery, \mathcal{E}_{SPR} .

Table 4 shows the estimate $Q(\mathbf{e}_{es}) = \mathcal{E}_{\text{SPR-CX}}$, the exact error $Q(\mathbf{e})$, the effectivity index for the QoI θ_{QoI} and the effectivity of the error estimator θ . For this problem the exact value of the QoI is $\bar{\sigma}_x = 0.06$. Table 4 indicates that the equilibrated recovery procedure (SPR-CX) provides very accurate estimations of the error in the QoI and in the value of the QoI itself, with $\theta = 1.0259$ and $\theta_{QoI} = 1.00000063$ for 79442 dof.

Table 4: Problem 1.d. Values for the error estimate $\mathcal{E}_{\text{SPR-CX}}$ and effectivities.

dof	$Q(\mathbf{e}_{es}) = \mathcal{E}_{\text{SPR-CX}}$	$Q(\mathbf{e})$	θ	θ_{QoI}
528	$1.659077 \cdot 10^{-3}$	$1.738923 \cdot 10^{-3}$	0.95408307	1.00119769
1,350	$8.225557 \cdot 10^{-5}$	$7.687113 \cdot 10^{-5}$	1.07004501	1.00008077
5,131	$2.678276 \cdot 10^{-5}$	$3.016986 \cdot 10^{-5}$	0.88773219	0.99994919
19,573	$1.108891 \cdot 10^{-5}$	$1.131773 \cdot 10^{-5}$	0.97978268	0.99999657
79,442	$1.655151 \cdot 10^{-6}$	$1.613254 \cdot 10^{-6}$	1.02597049	1.00000063

6.2 Problem 2: L-Shape plate

Let us consider the singular problem of a finite portion of an infinite domain with a reentrant corner. The model is loaded on the boundary with the tractions corresponding to the first terms of the asymptotic expansion that describes the exact solution under mixed mode loading conditions around the singular vertex, see Figure 15. The exact values of boundary tractions on the boundaries represented by discontinuous thick lines have been imposed in the FE analyses.

The exact displacement and stress fields for this singular elasticity problem can be found in [33]. Exact values of the generalised stress intensity factors (GSIF) [33] under mixed mode have been taken as $K_I = 1$ and $K_{II} = 1$. The material parameters are Young's modulus $E = 1000$, and Poisson's ratio $\nu = 0.3$. As

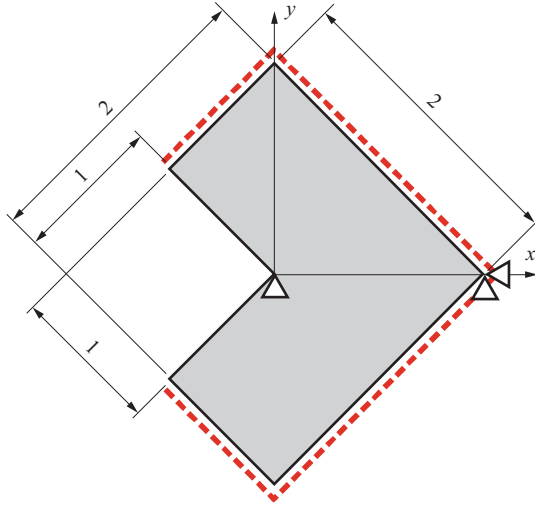


Figure 15: Problem 2. L-shaped domain.

the analytical solution of this problem is singular at the reentrant corner of the plate, for the recovery of the dual and primal fields we apply the *singular+smooth* decomposition of the stresses as explained in Section 5. We utilise a domain integral method based on extraction functions to obtain an approximation of the recovered singular part as explained in Section 5.

In this example, we consider the GSIFs K_I and K_{II} as the quantities of interest. Figure 16 shows the Cartesian meshes used to solve the primal and dual problems. For the dual problem, we use the same Dirichlet conditions as shown in Figure 15 and the set of nodal forces used to extract the QoI in the annular domain Ω_i , defined by a plateau function q , shown in Figure 16. Function q is defined such that $q = 1$ for $r \leq 0.6$, $q = 0$ for $r \geq 0.8$ and has a smooth transition for $0.6 < r < 0.8$ given by a quartic spline $1 - 6s^2 + 8s^3 - 3s^4$.

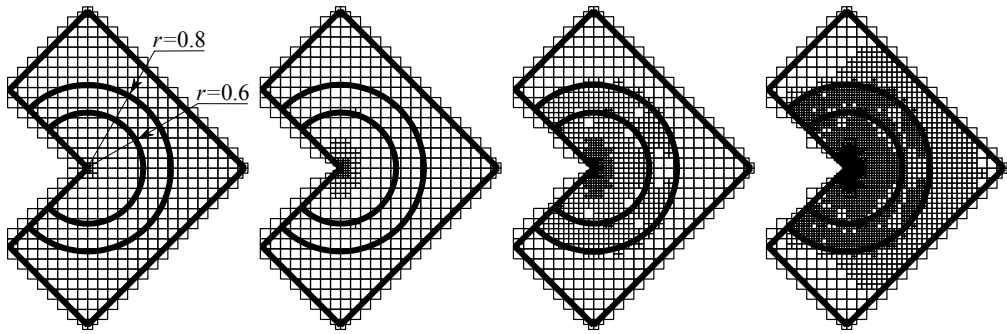


Figure 16: Problem 2. Cartesian meshes with h -adaptive refinement.

In order to impose equilibrium conditions during the recovery of the stresses we use the following approach. For the primal solution, in each patch, we enforce internal equilibrium and compatibility in Ω , and boundary equilibrium all along the Neumann boundary. For the dual problem, we enforce internal equilibrium using the initial strains and body loads shown in (44) and homogeneous Neumann boundary conditions. Compatibility is enforced within all the domain.

Table 5: Problem 2. Stress intensity factor K_I as QoI using initial strains formulation.

dof	$Q(\mathbf{e}_{es}) = \mathcal{E}_{\text{SPR-CX}}$	$Q(\mathbf{e})$	θ	θ_{QoI}
1,101	$7.302834 \cdot 10^{-3}$	$9.566751 \cdot 10^{-3}$	0.76335570	0.99773608
2,927	$2.065838 \cdot 10^{-3}$	$2.206343 \cdot 10^{-3}$	0.93631774	0.99985950
10,399	$5.194502 \cdot 10^{-4}$	$5.280162 \cdot 10^{-4}$	0.98377707	0.99999143
39,193	$1.300133 \cdot 10^{-4}$	$1.307862 \cdot 10^{-4}$	0.99409058	0.99999923

Table 6: Problem 2. Stress intensity factor K_{II} as QoI using initial strains formulation.

dof	$Q(\mathbf{e}_{es}) = \mathcal{E}_{\text{SPR-CX}}$	$Q(\mathbf{e})$	θ	θ_{QoI}
1,101	$2.031449 \cdot 10^{-3}$	$1.797716 \cdot 10^{-3}$	1.13001659	1.00023373
2,927	$5.273469 \cdot 10^{-4}$	$4.342458 \cdot 10^{-4}$	1.21439713	1.00009310
10,399	$1.013432 \cdot 10^{-4}$	$9.947112 \cdot 10^{-5}$	1.01881993	1.00000187
39,193	$2.440128 \cdot 10^{-5}$	$2.387141 \cdot 10^{-5}$	1.02219675	1.00000053

Table 5 shows the results for the stress intensity factor K_I . Similarly to the results for other QoIs, we observe that the proposed technique provides an accurate estimate $Q(\mathbf{e}_{es})$ of the exact error $Q(\mathbf{e})$. The effectivity index θ is always close to the optimal value $\theta = 1$ and for the last mesh with 39,193 dof we obtain $\theta = 0.9940$. As a result, and in agreement with the previous cases, the effectivity in the QoI is highly accurate, with $\theta_{QoI} = 0.9999$ for the same mesh. Table 6 shows the same results for the stress intensity factor K_{II} . Again, we observe a satisfactory behaviour of the error indicator and very accurate effectivities, both for the error estimate and for the QoI itself ($\theta = 1.0222$ and $\theta_{QoI} = 1.0$ for the last mesh).

Figure 17 shows the evolution of the relative error with respect to the number of dof for the two QoIs. Figures 18 and 19 show the evolution of the effectivity index of the error estimators obtained with the locally equilibrated SPR-CX technique, and with the non-equilibrated recovery as we increase the number of dof. The results indicate that the proposed methodology accurately evaluates the error in the QoI, giving values of θ close to 1 and considerably improving the results obtained with the original SPR technique (for the finest mesh considering K_{II} we have $\theta = 0.8610$ for the standard SPR and $\theta = 1.0222$ for the SPR-CX).

7 Conclusions and future work

In this paper, we present an *a posteriori* recovery-based strategy that aims to control the error in quantities of interest. The proposed technique is based on the use of a recovery procedure that considers locally equilibrated stress fields for both the primal and the dual problem.

To recover the solution for the primal problem the formulation considers the enforcement of equilibrium and compatibility equations, and the splitting of the FE field for singular problems [15]. In order to enforce equilibrium conditions when

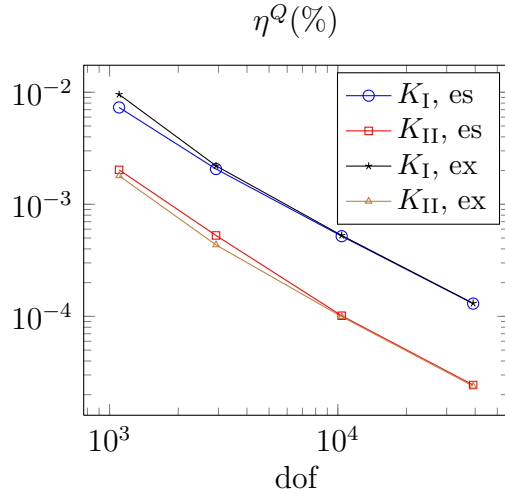


Figure 17: Problem 2. Evolution of the relative error η^Q for QoIs K_I and K_{II} , for the exact and estimated error as defined in (55).

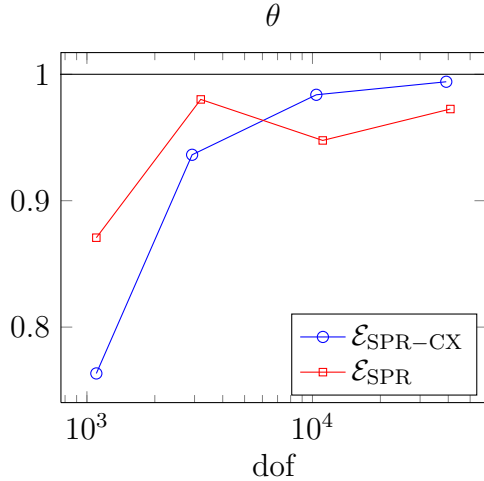


Figure 18: Problem 2. Evolution of the effectivity index θ for K_I

evaluating the recovered stress fields for the dual problem, we have considered an approach that allows to express the functional which defines some QoIs in terms of body loads and boundary tractions applied to the dual problem. The proposed technique was tested on different quantities of interest: mean displacements and stresses on a domain of interest, mean displacements and tractions along a boundary and the generalised stress intensity factor in the singular problem of a reentrant corner.

The methodology we proposed provides accurate global and local evaluations of the error in the different quantities of interest analysed, improving the results obtained with the original SPR technique, whose satisfactory estimation of the global error can be attributed to compensating errors. In particular, our approach proves superior to the standard SPR when considering the local error.

An extension of the work presented here for extended finite element approxima-

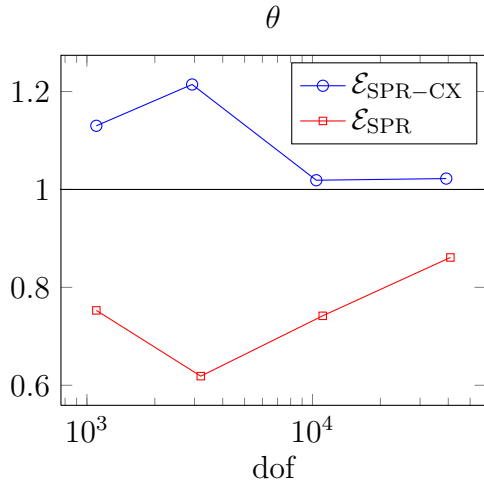


Figure 19: Problem 2. Evolution of the effectivity index θ for K_{II}

tions is now under development. The final goal is to be able to guide the adaptive process in 3D XFEM problems modelling fatigue crack growth using the stress intensity factors as design parameters for industrial applications of the XFEM similar to those discussed in the early work of References [56] [57], [58] and [59, 60].

8 Acknowledgements

This work was supported by the EPSRC grant EP/G042705/1 “Increased Reliability for Industrially Relevant Automatic Crack Growth Simulation with the eXtended Finite Element Method”.

Stéphane Bordas also thanks partial funding for his time provided by the European Research Council Starting Independent Research Grant (ERC Stg grant agreement No. 279578) “RealTCut Towards real time multiscale simulation of cutting in non-linear materials with applications to surgical simulation and computer guided surgery”.

This work has received partial support from the research project DPI2010-20542 of the Ministerio de Economía y Competitividad (Spain). The financial support of the FPU program (AP2008-01086), the funding from Universitat Politècnica de València and Generalitat Valenciana (PROMETEO/2012/023) are also acknowledged.

All authors also thank the partial support of the Framework Programme 7 Initial Training Network Funding under grant number 289361 “Integrating Numerical Simulation and Geometric Design Technology.”

References

[1] Ainsworth M, Oden JT. *A posteriori Error Estimation in Finite Element Analysis*. John Wiley & Sons: Chichester, 2000.

- [2] Stein E, Ramm E, Rannacher R. *Error-controlled adaptive finite elements in solid mechanics*. Wiley: Chichester, 2003.
- [3] Babuška I, Rheinboldt WC. A-posteriori error estimates for the finite element method. *International Journal for Numerical Methods in Engineering* 1978; **12**(10):1597–1615.
- [4] Zienkiewicz OC, Zhu JZ. A simple error estimator and adaptive procedure for practical engineering analysis. *International Journal for Numerical Methods in Engineering* 1987; **24**(2):337–357.
- [5] Zienkiewicz OC, Zhu JZ. The superconvergent patch recovery and a posteriori error estimates. Part 1: The recovery technique. *International Journal for Numerical Methods in Engineering* 1992; **33**(7):1331–1364.
- [6] Zienkiewicz OC, Zhu JZ. The superconvergent patch recovery and a posteriori error estimates. Part 2: Error estimates and adaptivity. *International Journal for Numerical Methods in Engineering* 1992; **33**(7):1365–1382.
- [7] Wiberg NE, Abdulwahab F. Patch recovery based on superconvergent derivatives and equilibrium. *International Journal for Numerical Methods in Engineering* Aug 1993; **36**(16):2703–2724.
- [8] Wiberg NE, Abdulwahab F, Ziukas S. Enhanced superconvergent patch recovery incorporating equilibrium and boundary conditions. *International Journal for Numerical Methods in Engineering* Oct 1994; **37**(20):3417–3440.
- [9] Ramsay ACA, Maudner EAW. Effective error estimation from continuous, boundary admissible estimated stress fields. *Computers & Structures* Oct 1996; **61**(2):331–343.
- [10] Kvamsdal T, Okstad KM. Error estimation based on Superconvergent Patch Recovery using statically admissible stress fields. *International Journal for Numerical Methods in Engineering* Jun 1998; **42**(3):443–472.
- [11] Xiao QZ, Karihaloo BL. Improving the accuracy of XFEM crack tip fields using higher order quadrature and statically admissible stress recovery. *International Journal for Numerical Methods in Engineering* 2006; **66**(9):1378–1410.
- [12] Ródenas JJ, Tur M, Fuenmayor FJ, Vercher A. Improvement of the superconvergent patch recovery technique by the use of constraint equations: the SPR-C technique. *International Journal for Numerical Methods in Engineering* 2007; **70**(6):705–727.
- [13] Bordas SPA, Duflot M. Derivative recovery and a posteriori error estimate for extended finite elements. *Computer Methods in Applied Mechanics and Engineering* 2007; **196**(35-36):3381–3399.
- [14] Bordas SPA, Duflot M, Le P. A simple error estimator for extended finite elements. *Communications in Numerical Methods in Engineering* 2008; **24**(11):961–971.

- [15] Ródenas JJ, González-Estrada OA, Tarancón JE, Fuenmayor FJ. A recovery-type error estimator for the extended finite element method based on singular+smooth stress field splitting. *International Journal for Numerical Methods in Engineering* 2008; **76**(4):545–571.
- [16] Duflot M, Bordas SPA. A posteriori error estimation for extended finite elements by an extended global recovery. *International Journal for Numerical Methods in Engineering* 2008; **76**:1123–1138.
- [17] González-Estrada O, Natarajan S, Ródenas J, Nguyen-Xuan H, Bordas S. Efficient recovery-based error estimation for the smoothed finite element method for smooth and singular linear elasticity. *Computational Mechanics* 2012; :1–16.
- [18] González-Estrada O, Ródenas J, Bordas S, Duflot M, Kerfriden P, Giner E. On the role of enrichment and statical admissibility of recovered fields in a-posteriori error estimation for enriched finite element methods. *Engineering Computations* 2012; **29**(8):2–2.
- [19] Pereira OJBA, de Almeida JPM, Maunder EAW. Adaptive methods for hybrid equilibrium finite element models. *Computer Methods in Applied Mechanics and Engineering* Jul 1999; **176**(1-4):19–39.
- [20] Paraschivoiu M, Peraire J, Patera AT. A posteriori finite element bounds for linear-functional outputs of elliptic partial differential equations. *Computer Methods in Applied Mechanics and Engineering* 1997; **150**(1-4):289–312.
- [21] Ladevèze P, Rougeot P, Blanchard P, Moreau JP. Local error estimators for finite element linear analysis. *Computer Methods in Applied Mechanics and Engineering* 1999; **176**(1-4):231–246.
- [22] Oden JT, Prudhomme S. Goal-oriented error estimation and adaptivity for the finite element method. *Computers & Mathematics with Applications* Mar 2001; **41**(5-6):735–756.
- [23] Cirak F, Ramm E. A posteriori error estimation and adaptivity for linear elasticity using the reciprocal theorem. *Computer Methods in Applied Mechanics and Engineering* Apr 1998; **156**(1-4):351–362.
- [24] Rüter M, Stein E. Goal-oriented a posteriori error estimates in linear elastic fracture mechanics. *Computer Methods in Applied Mechanics and Engineering* Jan 2006; **195**(4-6):251–278.
- [25] de Almeida JPM, Pereira OJBA. Upper bounds of the error in local quantities using equilibrated and compatible finite element solutions for linear elastic problems. *Computer Methods in Applied Mechanics and Engineering* Jan 2006; **195**(4-6):279–296.
- [26] Díez P, Ródenas JJ, Zienkiewicz OC. Equilibrated patch recovery error estimates: simple and accurate upper bounds of the error. *International Journal for Numerical Methods in Engineering* 2007; **69**(10):2075–2098.

- [27] Ródenas JJ, González-Estrada OA, Díez P, Fuenmayor FJ. Accurate recovery-based upper error bounds for the extended finite element framework. *Computer Methods in Applied Mechanics and Engineering* 2010; **199**(37-40):2607–2621.
- [28] Verfürth R. A review of a posteriori error estimation techniques for elasticity problems. *Computer Methods in Applied Mechanics and Engineering* 1999; **176**:419–440.
- [29] Blacker T, Belytschko T. Superconvergent patch recovery with equilibrium and conjoint interpolant enhancements. *International Journal for Numerical Methods in Engineering* 1994; **37**(3):517–536.
- [30] Ródenas JJ. Goal Oriented Adaptivity: Una introducción a través del problema elástico lineal. *Technical Report*, CIMNE, PI274, Barcelona, Spain 2005.
- [31] González-Estrada OA, Ródenas JJ, Nadal E, Bordas SPA, Kerfriden P. Equilibrated patch recovery for accurate evaluation of upper error bounds in quantities of interest. *Adaptive Modeling and Simulation. Proceedings of V ADMOS 2011*, Aubry D, Díez P, Tie B, Parés N (eds.), CIMNE: Paris, 2011.
- [32] Verdugo F, Díez P, Casadei F. Natural quantities of interest in linear elastodynamics for goal oriented error estimation and adaptivity. *Adaptive Modeling and Simulation. Proceedings of V ADMOS 2011*, Aubry D, Díez P, Tie B, Parés N (eds.), CIMNE: Paris, 2011.
- [33] Szabó BA, Babuška I. *Finite Element Analysis*. John Wiley & Sons: New York, 1991.
- [34] Ródenas JJ, Giner E, Tarancón JE, González-Estrada OA. A recovery error estimator for singular problems using singular+smooth field splitting. *Fifth International Conference on Engineering Computational Technology*, Topping BHV, Montero G, Montenegro R (eds.), Civil-Comp Press: Stirling, Scotland, 2006.
- [35] González-Estrada OA, Nadal E, Ródenas JJ, Kerfriden P, Bordas SPA. Error estimation in quantities of interest for XFEM using recovery techniques. *20th UK National Conference of the Association for Computational Mechanics in Engineering (ACME)*, Yang ZJ (ed.), The University of Manchester: Manchester, 2012; 333–336.
- [36] Pannachet T, Sluys LJ, Askes H. Error estimation and adaptivity for discontinuous failure. *International Journal for Numerical Methods in Engineering* 2009; **78**(5):528–563.
- [37] Giner E, Tur M, Fuenmayor FJ. A domain integral for the calculation of generalized stress intensity factors in sliding complete contacts. *International Journal of Solids and Structures* Feb 2009; **46**(3-4):938–951.
- [38] Nadal E, Ródenas JJ, Tarancón JE, Fuenmayor FJ. On the advantages of the use of cartesian grid solvers in shape optimization problems. *Adaptive Modeling and Simulation. Proceedings of V ADMOS 2011*, Aubry D, Díez P, Tie B, Parés N (eds.), CIMNE: Paris, 2011.

[39] Moumnassi M, Belouettar S, Béchet E, Bordas SPA, Quoirin D, Potier-Ferry M. Finite element analysis on implicitly defined domains: An accurate representation based on arbitrary parametric surfaces. *Computer Methods in Applied Mechanics and Engineering* Jan 2011; **200**(5-8):774–796.

[40] Belytschko T, Parimi C, Moës N, Sukumar N, Usui S. Structured extended finite element methods for solids defined by implicit surfaces. *International Journal for Numerical Methods in Engineering* Jan 2003; **56**(4):609–635.

[41] Moës N, Cloirec M, Cartraud P, Remacle JF. A computational approach to handle complex microstructure geometries. *Computer Methods in Applied Mechanics and Engineering* Jul 2003; **192**(28-30):3163–3177.

[42] Gordon WJ, Hall CA. Construction of curvilinear co-ordinate systems and applications to mesh generation. *International Journal for Numerical Methods in Engineering* 1973; **7**(4):461–477.

[43] Sevilla R, Fernández-Méndez S. NURBS-enhanced finite element method (NE-FEM). *Online* 2008; **76**(1):56–83.

[44] Béchet E, Moës N, Wohlmuth B. A stable Lagrange multiplier space for stiff interface conditions within the extended finite element method. *International Journal for Numerical Methods in Engineering* 2009; **78**:931–954.

[45] Menk A, Bordas S. A robust preconditioning technique for the extended finite element method. *International Journal for Numerical Methods in Engineering* 2011; **85**(13):1609–1632.

[46] Schweitzer M. Stable enrichment and local preconditioning in the particle-partition of unity method. *Numerische Mathematik* 2011; **118**(1):137–170.

[47] Hiriyur B, Tuminaro R, Waisman H, Boman E, Keyes D. A quasi-algebraic multigrid approach to fracture problems based on extended finite elements. *SIAM Journal on Scientific Computing* 2012; **34**(2):603–626.

[48] Gerstenberger A, Tuminaro R. An algebraic multigrid approach to solve xfem based fracture problems 2012.

[49] Ladevèze P, Marin P, Pelle JP, Gastine JL. Accuracy and optimal meshes in finite element computation for nearly incompressible materials. *Computer Methods in Applied Mechanics and Engineering* 1992; **94**(3):303–315.

[50] Coorevits P, Ladevèze P, Pelle JP. An automatic procedure with a control of accuracy for finite element analysis in 2D elasticity. *Computer Methods in Applied Mechanics and Engineering* 1995; **121**:91–120.

[51] Ladevèze P, Leguillon D. Error estimate procedure in the finite element method and applications. *SIAM Journal on Numerical Analysis* 1983; **20**(3):485–509.

- [52] Li LY, Bettess P. Notes on mesh optimal criteria in adaptive finite element computations. *Communications in Numerical Methods in Engineering* 1995; **11**(11):911–915.
- [53] Fuenmayor FJ, Oliver JL. Criteria to achieve nearly optimal meshes in the h-adaptive finite element method. *International Journal for Numerical Methods in Engineering* 1996; **39**:4039–4061.
- [54] Abel JF, Shephard MS. An algorithm for multipoint constraints in finite element analysis. *International Journal for Numerical Methods in Engineering* 1979; **14**(3):464–467.
- [55] Farhat C, Lacour C, Rixen D. Incorporation of linear multipoint constraints in substructure based iterative solvers. Part 1: a numerically scalable algorithm. *International Journal for Numerical Methods in Engineering* 1998; **43**(6):997–1016.
- [56] Bordas SPA, Moran B. Enriched finite elements and level sets for damage tolerance assessment of complex structures. *Engineering Fracture Mechanics* Jun 2006; **73**(9):1176–1201.
- [57] Bordas S, Conley J, Moran B, Gray J, Nichols E. A simulation-based design paradigm for complex cast components. *Engineering with Computers* 2007; **23**(1):25–37.
- [58] Bordas SPA, Nguyen PV, Dunant C, Guidoum A, Nguyen-Dang H. An extended finite element library. *International Journal for Numerical Methods in Engineering* 2007; **71**(6):703–732.
- [59] Wyart E, Coulon D, Duflot M, Pardoen T, Remacle JF, Lani F. A substructured FE-shell/XFE-3D method for crack analysis in thin-walled structures. *International Journal for Numerical Methods in Engineering* 2007; **72**(7):757–779.
- [60] Wyart E, Duflot M, Coulon D, Martiny P, Pardoen T, Remacle JF, Lani F. Substructuring FEXFE approaches applied to three-dimensional crack propagation. *Journal of Computational and Applied Mathematics* Jun 2008; **215**(2):626–638.